An Experimental Study on Heat Transfer Characteristics of Porous Media Subjected to Submerged Two-Phase Jet Impingement

by

Matthew C. Hull

Submitted in Partial Fulfillment of the Requirements

for the Degree of

Master of Science in Engineering

In

Mechanical Engineering

YOUNGSTOWN STATE UNIVERSITY

May, 2024

An Experimental Study on Heat Transfer Characteristics of Porous Media Subjected to Submerged Two-Phase Jet Impingement

Matthew C. Hull

I hereby release this thesis to the public. I understand that this thesis will be made available from the OhioLINK ETD Center and the Maag Library Circulation Desk for public access. I also authorize the University or other individuals to make copies of this thesis as needed for scholarly research.

Signature:

_____

Matthew C. Hull, Student Date

Approvals:

_____

Kyosung Choo, PhD, Thesis Advisor Date

_____

Alexander Pesch, PhD, Committee Member Date

_____

Eric Haake, M.S.E, Committee Member Date

_____

Salvatore A. Sanders, PhD, Dean, College of Graduate Studies Date

Abstract

With the constant innovation of technology and the need for more power generation, the need for improved methods of heat transfer are also needed. These innovations have always driven the research into new and improved methods of heat transfer. The topics covered in this research mainly being porous media, submerged two-phase jet impingement and boiling have all been seen to create improvements in cooling but have not been used in conjunction with each other. Using this combination to find the possible heat transfer improvement is the goal of this research. Experiments are done in both a non-boiling and boiling scenario. This allowed for verification that the two-phase flow had an effect on the surface before performing a boiling experiment. Two surfaces were tested, these were a plain surface and a columnar post-wick porous structure. For both sets of experiments, water flow rates were chosen from Reynolds numbers of 729 and 2929. The air flow rates were calculated using values of the volumetric quality (β) that ranged from $0 \leq \beta \leq 0.9$ and the previously mentioned water flow rates. The results of this experiment were quantified by looking at the heat transfer coefficient (HTC) compared to the change in volumetric quality for both experiments. The non-boiling experiment showed that the added two-phase impinging jet created improvements in the HTC of porous media. An improvement of 81.94% over a single-phase jet was observed at a volumetric quality of $\beta = 0.9$. The boiling experiment showed that the added two-phase impinging jet made minimal improvements on each surface. The plain surface saw an improvement of 9.50% over a single-phase jet at a volumetric quality of $\beta = 0.9$. The post-wick surface saw a maximum improvement of only 2.94% at a volumetric quality of $\beta = 0.7$.

Table of Contents

Acknowledgements

First, I would like to thank my thesis adviser, Dr. Choo. The guidance you have given me has been very rewarding and educational. I appreciate all the time, advice, and work you have put into helping me complete my graduate studies. I would also like to thank my committee members, Dr. Pesch and Mr. Haake. Thank you both for the support and guidance during my studies. I would also like to thank the rest of the YSU Mechanical Engineering faculty for their guidance and support during my time at YSU.

Second, I would like to thank the Graduate College and Mechanical Engineering department for granting me a Graduate Assistantship throughout my studies. This assistantship allowed for me to solely focus on my studies and advancing my education, and for that I am grateful.

Lastly, I would like to thank Coleman Buchanan for his help in capturing the microscopic images shown in this research. I would also like to thank the rest of my friends for their continued support throughout this entire process. As for my family, you have always been supportive of my educational endeavors, and I am truly grateful for that support, so thank you for everything.

List of Figures

List of Tables

Nomenclature

Variables

β	Volumetric Quality
$\dot{Q}$	Heat Transfer Rate
k	Thermal Conductivity
A	Area
T	Temperature
$\dot{q}$	Heat Flux
ρ	Density
c_p	Specific Heat
μ	Dynamic Viscosity
u	Fluid Velocity
h	Convective Heat Transfer Coefficient
L	Length
Nu	Nusselt Number
$\dot{q}_{boiling}$	Nucleate Boiling Heat Flux
C	Experimental Constant Based on Heater Geometry
h_{fg}	Enthalpy of Vaporization
σ	Surface Tension of Liquid-Vapor Interface
g	Gravitational Acceleration
D	Diameter

Y	Mass Fraction
J	Diffusional Mass Flux
δ	Unit Tensor
τ	Viscous Stress Tensor
E	Total Energy
d	Nozzle Diameter
H	Nozzle-to-Plate Spacing
λ	Instability Wavelength
Q	Volumetric Flow Rate
j	Volumetric Flux (Superficial Velocity)
mm	Millimeters
in	Inches
µm	Micron
V	Volts
°C	Celsius
cc	Cubic Centimeter
min	Minute

Subscript

Cond	Conduction Heat Transfer
Conv	Convection Heat Transfer
s	Surface
∞	Ambient

c	Characteristic
sat	Saturation
max	Maximum
min	Minimum
cr	Critical Heat Flux Constant
v	Vapor
g	Gas
l	Liquid
$film$	Film Boiling
0	Stagnation
f	Flow
p	Phase or Pitch
RT	Rayleigh-Taylor
ps	Plain Surface
cp	Columnar Post
β	Volumetric Quality

Superscripts

$*$	Normalized Value

Acronyms

HTC	Heat Transfer Coefficient
CHF	Critical Heat Flux

LPS	Lattice Porous Structure

Chapter 1 - Introduction

1.1 - Problem Statement

With the constant innovation of technology, like the advances in electronics and electric vehicles, more emphasis is placed on the use and generation of more power. This increase in power creates the need for advanced methods of heat transfer and the need for this area of research. All the aspects of this research, the impinging jet, porous media, and the two-phase flow, are known to improve the effects of heat transfer. Jet impingement has been implemented in a range of technology from aerospace to steel mills, due to its high heat and mass transfer abilities [1]. Porous media allow for an increase of the HTC due to the increased fluid contact area and are commonly used in boiling scenarios as well as heat exchangers [2]. Two-phase flow is a common phenomenon that occurs in the cooling of nuclear reactors due to its high heat transfer rates caused by the turbulent mixing of the two phases. This combination of heat transfer methods may lead to an applicable enhancement of heat transfer.

This research will investigate the combination of two-phase jet impingement and porous media with the goal of achieving an enhancement of heat transfer. The results of this research will explore a non-boiling and boiling experiment within a submerged pool using a two-phase impinging jet. The submerged pool was chosen to replicate the pool-boiling effect and allowed for a method of verification. In both cases, Reynolds numbers

of 732 and 2929 were chosen and are discussed further, later in this report. Conclusions will be drawn about the HTC in both the non-boiling and boiling cases as a change in the volumetric quality occurs. The motivation behind this research was to build off former work on the topic of two-phase jet impingement and porous media, but no recent research explores the combination of the two methods.

Chapter 2 - Background

2.1 - Heat Transfer

Heat transfer and thermodynamics are two sub-disciplines of thermal engineering. While thermodynamics is looking at the total amount of energy transfer overall, heat transfer is dealing with the different methods of heat transport as well as the rate at which the energy is transferred. Engineers are commonly dealing with this rate of energy transfer as it is needed to properly design some cooling or heating applications. The methods of heat transport are normally broken down into three primary mechanisms, conduction, convection, and radiation. This thesis will focus on the primary mechanisms of conduction and convection.

2.1.1 - Conduction

Conduction deals with the energy transfer between adjacent particles of different energy levels. This energy flows from particles of more energy to particles of less, which is seen in the transfer of heat flowing from hot to colder mediums. Conduction can occur if energetic particles are present, meaning it can occur in solids, liquids, and gases. Within liquids and gases, conduction is performed by the effects of collisions and diffusions of molecules in random motion. Within solids, conduction is completed due to the combination of molecular vibrations within a lattice structure and the energy transport of free electrons. The rate of head conduction is affected by the geometry, thickness, and type of medium, as well as the temperature difference across it. Heat conduction was first

modeled by Joseph Fourier in 1822 within his book "The Analytical Theory of Heat" [3]. Fourier's law of heat conduction can be seen Equation (2.1).

$$\dot{Q}_{cond} = -kA\frac{dT}{dx} \tag{2.1}$$

Shown in Equation (2.1), $\frac{dT}{dx}$ is the temperature gradient across the medium, k is the thermal conductivity of the medium, and A is the heat conduction area. With Fourier's law, the negative sign ensures that heat flowing in the positive x-direction has a positive quantity. A general form of the heat conduction form can be seen in Equation (2.2) that accounts for variable thermal conductivity within a rectangular coordinate system.

$$\frac{\partial}{\partial x}\left(k\frac{\partial T}{\partial x}\right) + \frac{\partial}{\partial y}\left(k\frac{\partial T}{\partial y}\right) + \frac{\partial}{\partial z}\left(k\frac{\partial T}{\partial z}\right) + \dot{q} = \rho c_p \frac{\partial T}{\partial t} \tag{2.2}$$

It can be noted from Equation (2.2), that the general heat conduction equation is time dependent. With this, assumptions can be made of one-dimensional conduction and steady state conditions which generates Equation (2.3).

$$\dot{Q}_{cond} = kA\frac{T_1 - T_2}{\Delta x} \tag{2.3}$$

2.1.2 - Convection

Convection is another mechanism of heat transfer. It can be defined as the transfer of energy between a solid surface and the adjacent fluid that is in motion. This mechanism involves the effects of both conduction and fluid motion, which complicates the determination of the heat transfer rate. Based on the type of fluid motion in contact with the solid surface, the type of convection can be broken down into two different regimes, forced and natural. Natural (or free) convection is observed when no additional fluid motion is occurring across the surface and buoyancy effects of the surrounding fluid dictate the heat transfer rate. Forced convection requires some source of fluid motion, for example flowing water or wind. Convection can also be classified as internal or external based on the type of system the heat is being transferred in. In an internal case, flow is within the boundary of some geometry, like a pipe or duct work. As for the external case, flow is being moved around the surface of an object. Various types of experimental work have been documented showing that changing the fluid parameters or properties have an impact on the overall convective heat transfer [4, 5, 6]. Some examples of changed parameters are the dynamic viscosity μ, thermal conductivity k, density ρ, specific heat c_p, and fluid velocity u. Along with the different parameters of the fluid flow, convection is also affected by the geometry and other surface conditions. Newton created the law of cooling where the rate of convective heat transfer is a function of the surface area, temperature difference between the surface and surrounding fluid, as well as a heat transfer coefficient seen in Equation (2.4).

$$\dot{Q}_{conv} = hA_s(T_s - T_\infty) \tag{2.4}$$

The convection heat transfer coefficient, h in the above equation is a property of the entire heat transfer system and not of just the fluid or surface. Due to this, the coefficients' values must be determined experimentally in each unique case. This study will use the heat transfer coefficient to determine the effectiveness of the applied methods of heat transfer.

In some studies of convection effects, it is beneficial to denote the transfer of heat using a nondimensionalized number. This number is considered the Nusselt number. It is defined as being the ratio of the amount of convective heat transfer over the amount of conductive heat transfer. Its formulation can be seen in Equation (2.5), where h is the convective heat transfer coefficient, L_c is the characteristic length, and k is the thermal conductivity of the fluid.

$$Nu = \frac{hL_c}{k} \tag{2.5}$$

2.2 - Boiling

Boiling is a liquid-to-vapor phase change that occurs when a liquid encounters a surface that is held at a temperature at or above the saturation temperature of the fluid. It can be described as pool boiling in the absence of bulk fluid motion and flow boiling in the presence of it. The driving force of heat transfer due to boiling is the temperature difference

between the vapor in the bubbles and the surrounding liquid. At the solid-liquid interface, vapor bubbles form and detach from the surface and rise in the liquid. The bubbles will be too small and collapse within the liquid until the surface temperature rises and then the bubbles will rise until they reach the free surface. Since boiling is a form of convective heat transfer, the boiling heat flux can be expressed using Newton's law of cooling and can be seen in Equation (2.6).

$$\dot{q}_{boiling} = h(T_s - T_\infty) \tag{2.6}$$

The boiling heat flux and the excess temperature shown in the above equation are used to depict the boiling curve shown in Figure 2.1. Four different boiling regimes are depicted on the boiling curve. These regimes are natural convection boiling, nucleate boiling, transition boiling, and film boiling. These regimes can be broken down based on the excess temperature (the difference between the surface temperature and the saturation temperature of the fluid) and the boiling heat flux.

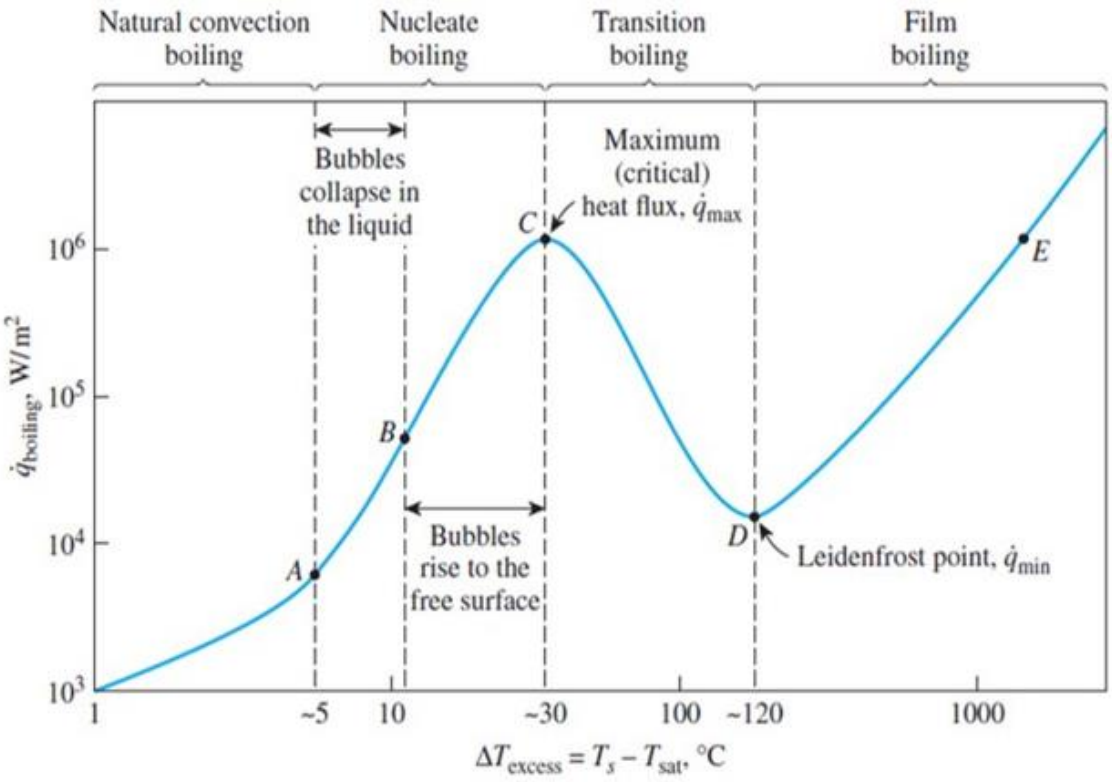

Figure 2.1: Boiling curve for water at 1 atm. [7]

The first boiling regime is the natural convection region. Here, the temperature of the heated surface is slightly above the saturation temperature of the liquid. Bubbles start to form at the solid-liquid interface, but do not detach from the surface. Within this regime natural convection currents perform the heat transfer and can be defined by natural convection laws.

The second regime is the nucleate boiling region. This regime has three key phenomena occur. First bubbles can be seen detaching from the surface and collapse within the fluid as can be seen from region *A* to *B* in Figure 2.1. Then from *B* to *C*, bubbles become large enough to rise to the free surface. Once the excess temperature reaches values closer

to that of point *C*, vapor columns will form within the liquid. These columns are caused by the large size of the bubbles and the high amount of nucleation sites on the surface. Multiple empirical correlations have been formed, but the most widely accepted was made by W.M. Rohsenow [7, 8, 9]. The correlation can be seen in the results and discussions chapter as Equation (4.1).

Then, at point *C* the critical heat flux (CHF) occurs. The critical heat flux, $\dot{q}_{max}$ is the point at which it becomes difficult for liquid to reach the heated surface due to the high rate of evaporation. Due to this, CHF is the highest amount of energy that can be removed from the system while maintaining a solid-liquid interface. Above this point surface dry-out occurs and heat transfer is then done through a solid-gas interface, which is far less effective. A theoretical correlation was formed by both S.S. Kutateladze and N. Zuber using two different approaches [7]. This correlation can be seen in Equation (2.7).

$$\dot{q}_{max} = C_{cr} h_{fg} [\sigma g \rho_v^2 (\rho_l - \rho_v)]^{\frac{1}{4}} \tag{2.7}$$

Transition boiling is the third boiling regime. Within this regime, the heat flux drastically drops due to the aforementioned solid-gas interface or vapor film. This vapor film acts as an insulator due to the low thermal conductivity of vapor. In most experiments this regime is missed due to the temperature of the surface rising rapidly above the saturation temperature of the liquid. The Leidenfrost point, $\dot{q}_{min}$, which is the lowest achievable heat flux that occurs during the boiling process. J.C. Leidenfrost observed this

phenomenon in 1756, when he saw liquid droplets on a very hot surface jump around and slowly boil away [7]. The correlation equation can be seen in Equation (2.8).

$$\dot{q}_{min} = 0.09\rho_v h_{fg}\left[\frac{\sigma g(\rho_l - \rho_v)}{(\rho_l - \rho_v)^2}\right]^{\frac{1}{4}} \quad (2.8)$$

The fourth boiling regime is film boiling. Film boiling will sometimes also be considered surface-dry out or burn out, since liquid cannot reach the heater surface and a layer or "film" of vapor is formed on the heater surface. Within this region radiation effects dominate the heat transfer in the system, so while the surface temperature increases, so does the heat flux. In 1950, Bromley [10] developed a theory on the prediction of stable film boiling heat transfer on the outside of a horizontal cylinder. His prediction of the heat flux in a stable film can be seen in Equation (2.9).

$$\dot{q}_{film} = C_{film}\left[\frac{g k_v^3 \rho_v(\rho_l - \rho_v)\left[h_{fg} + 0.4c_{pv}(T_s - T_{sat})\right]}{\mu_v D(T_s - T_{sat})}\right]^{\frac{1}{4}}(T_s - T_{sat}) \quad (2.9)$$

The relationships shown in Equations (2.7) through (2.9), and (4.1), are all developed from empirical correlation. These equations are assuming that fluid is in contact with a polished heating surface, which also assumes that the nucleation sites are occurring on the same sublevel as the fluid contacting the heater surface. Due to these equations being just correlations, they need to be used carefully as high levels of error are associated with them.

2.2.1 - Porous Media

One of the main issues with pool boiling is its limited heat transfer capability due to surface dry-out. Surface dry-out, as mentioned above, occurs when an inadequate amount of liquid can reach the heater surface. This is caused by the effect of a critical liquid-vapor hydrodynamic wavelength. This wavelength is also called the Rayleigh-Taylor instability wavelength. This wavelength can be defined as when a fluid of less density supports that of a higher density. This interface can become unstable if any disturbance occurs causing the higher density fluid to penetrate the less dense one [11]. The conservation equations between two miscible fluids are shown in Equation (2.10) through Equation (2.12). These equations were developed by Lord Rayleigh and Sir Geoffrey Ingram.

$$\frac{\partial \rho Y_i}{\partial t} + \nabla \cdot \left(\rho Y_i \vec{u} + \vec{J_l}\right) = 0; (i = 1, 2, 3 \ldots n) \qquad (2.10)$$

$$\frac{\partial \rho \vec{u}}{\partial t} + \nabla \cdot \left[\rho \vec{u} + p\vec{\delta} - \vec{\tau}\right] = \rho \vec{g} \qquad (2.11)$$

$$\frac{\partial E}{\partial t} + \nabla \cdot \left[(E + p)\vec{u} - \vec{\tau} \cdot \vec{u} + \vec{q}_{cond} + \vec{h}_{fg}\right] = \rho g \cdot \vec{u} \qquad (2.12)$$

Pool boiling is limited due to the increase in the hydrodynamic instability wavelength. This has led to an influx of research to better understand surface dry-out and to try and improve the HTC and CHF. One of the top topics being looked at to improve these statistics is that of porous media. Porous media are structures made up of very small

particles that allow for fluid flow between the particles. The structures are typically made of copper, ceramics, or other metals. Various shapes can be made with these as well, due to the small nature of the particles. Some examples of shapes include microchannels, mesh-like wicks, honeycomb structures, and different variations of posts (Columnar, Mushroom, etc.). These structures are typically used within heat exchangers and heat pipes but can also be created to work as heat sinks in most cases. The main benefit to their use is the high HTC they produce which greatly increases convective heat transfer.

Most modern research on this topic are focused on the application of numerical methods to determine the best geometry of porous structure [12, 13]. The changes in pore size and pore orientation among others have been investigated in trying to optimize the hydrodynamic wavelength. In numerical research, Xuan et al, looked at the effects of porosity, thermal conductivity of the fluid and solid surface, and heating direction on the critical pore size. They found that critical pore size decreases with increasing porosity and heating temperature but increases with the rise in thermal conductivity of the solid surface [14]. Experimental research has also been performed using porous and other microstructures [15, 16, 17, 18]. Miao et al [19], investigated the heat dissipation of an aluminum alloy lattice porous structure (LPS) that was subjected to an air impinging jet. They looked at various iterations of the lattice structure based on rod diameter and height which changed the porosity of each test piece. The results of their experimental tests can be seen in Figure 2.2. They found that as the height of the LPS increases, the Nusselt number increased and then decreased with an optimal height of 6mm. They also discovered that having a higher porosity at low pump power yields better performance and vice versa for lower porosity structures.

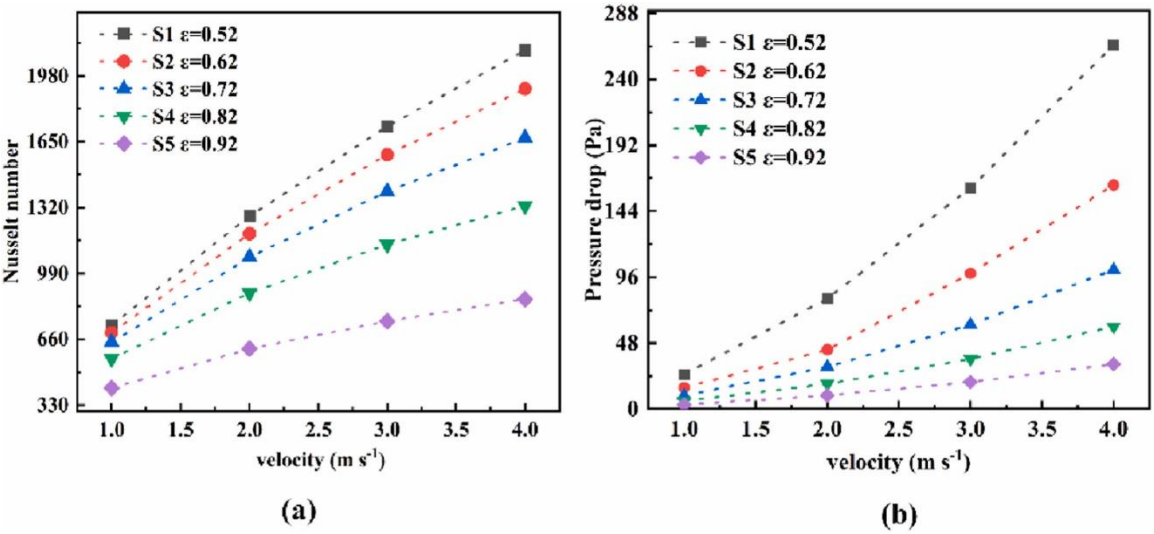

Figure 2.2: Variations in (a) Nusselt number and (b) pressure drop of LPS over changes in velocity and porosity [19].

Some more recent research looking directly on the effects of porous structures in boiling scenarios was performed by Nasersharifi et al. [20]. They designed their own multi-level modulated wicks out of sintered spherical particles having diameters of 200 μm. With these particles they made three surfaces, monolayer wick, post wick, and a mushroom wick which can be seen in Figure 2.3. Each of these surfaces was designed with a unique purpose in mind. The monolayer wick was designed to increase the HTC by decreasing the effective wick thickness. The post wick built on the back of the monolayer wick by also actively controlling the hydrodynamic instability wavelength using the distance between the pitches. The mushroom wick could also control wavelength but allowed for easier supply of liquid to the monolayer surface due to the increased surface area. Figure 2.4 shows the results of their experiment. Their experiment found that post wicks having a pitch distance

of 1mm resulted in the highest CHF, while the monolayer and mushroom posts created an improvement over a plain surface.

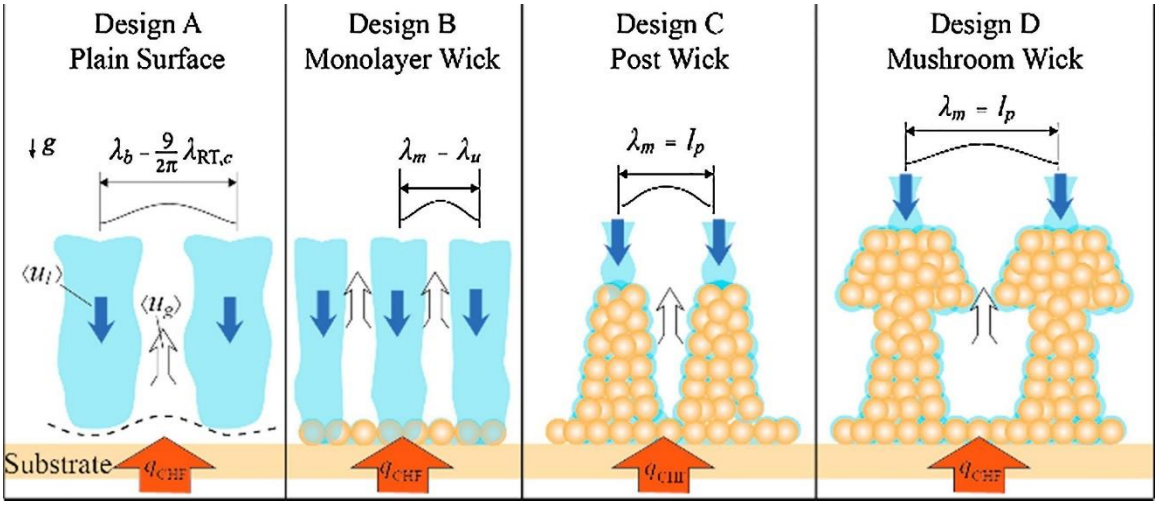

Figure 2.3: Schematic showing the different porous surfaces and there corresponding hydrodynamic instability wavelength. [20]

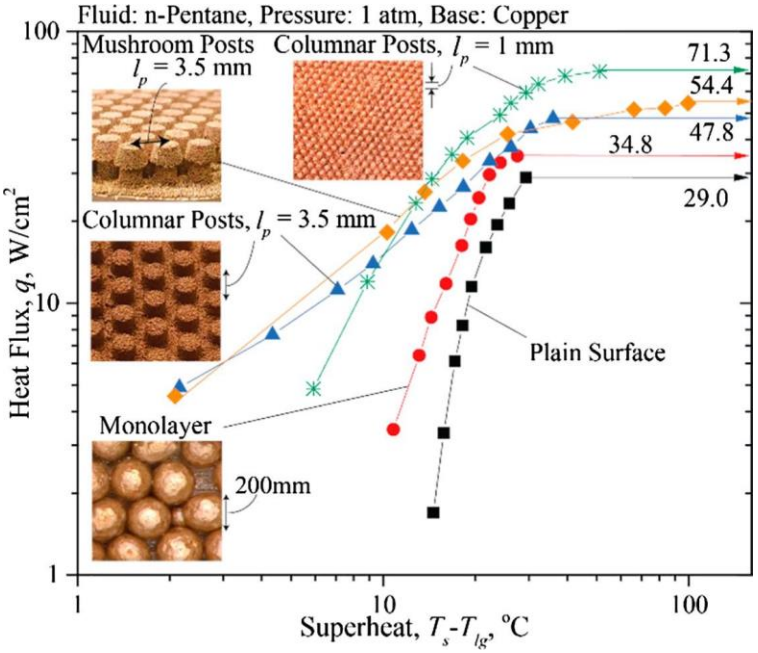

Figure 2.4: Heat flux vs wall superheat for all porous surfaces. [20]

This research by Nasersharifi was followed by the work of Bevan [21]. Bevan took the monolayer and post wick designs that were created by Nasersharifi and used them to create his own surfaces. Using these surfaces, he decided to add an impinging jet to try and improve the CHF and HTC. Using a pitch distance of 1mm, he found that based on the flow rate at which the impinging jet was at, the CHF had an improvement of 128% to 323% based on the surface being used. His results can be seen in Figure 2.5.

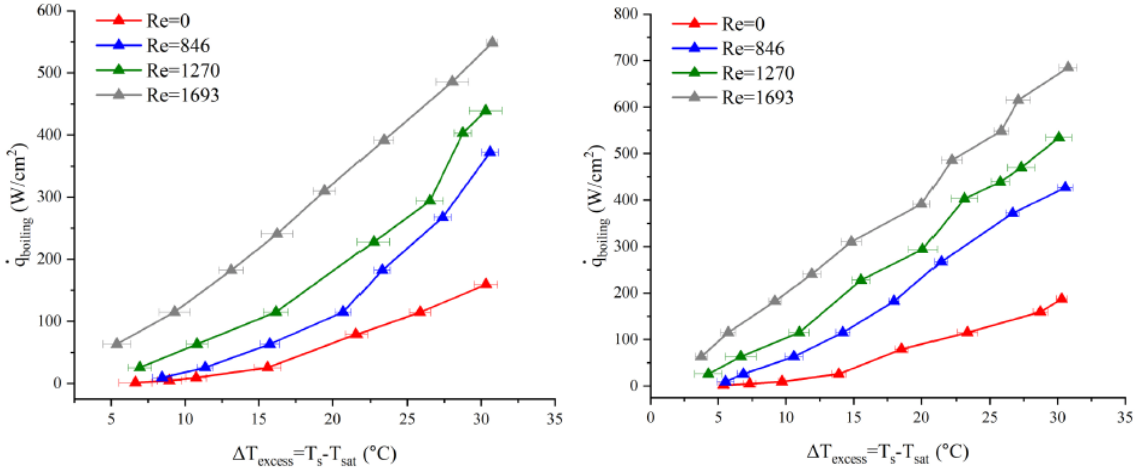

Figure 2.5: Effect on boiling curves for (a) monolayer wick and (b) post wick due to an impinging jet. [21]

2.3 - Impinging Jets

Impinging jets are highly valued due to their ability to offer high rates of both heat and mass transfer. Jet impingement can be defined as when a working fluid is sprayed onto a working surface. They are primarily used for cooling purposes but can also be used for

heating and drying applications. Some examples of uses of impinging jets include high-density electrical equipment cooling, quenching of metals, and vertical takeoff and landing of jets. The overall benefits of impinging jets come from the thin boundary layer of fluid that provides another method of heat transfer using convection. There are three common types of impinging jets, and these are free surface, submerged and confined. The research in this study is focused only on the submerged jet.

A free surface jet can be described as having no added boundary condition once leaving the nozzle. This can be considered as the fluid having a free condition where it can move in any which way it chooses. One effect that is created with a free surface jet is that of the hydraulic jump. This is the horizontal jet that is formed after the fluid contacts the surface. The main difference between a submerged jet and a free surface jet is the added wall boundary condition. Since the jet must be in a contained fluid to be described as submerged, the fluid exiting the nozzle will eventually contact a wall boundary. The previously mentioned hydraulic jump effect is not seen in the submerged case due to the fluid boundary. Figure 2.6 is a schematic of a submerged impinging jet showing its different features. The purpose of a submerged impinging jet is to expand the fluid boundary that is in contact with the surface. This expanded boundary generates a larger convection effect.

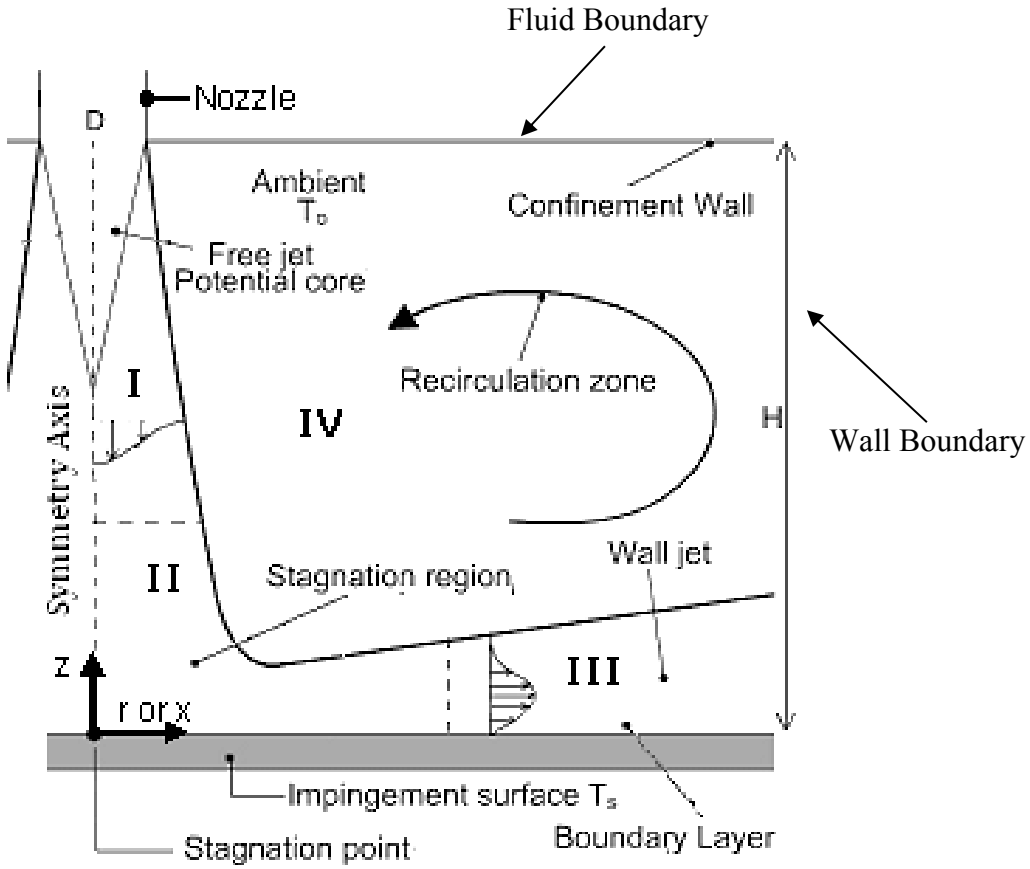

Figure 2.6: Schematic of a submerged impinging jet. [33]

In Figure 2.6 various key components of an impinging jet can be seen. D represents the diameter of the nozzle and Z, or H is the nozzle-to-plate spacing. This nozzle-to-plate spacing has been found to have considerable effects on the convective heat transfer, which will be discussed later. A stagnation point is created at the center of the impinging plate. Within a submerged jet a recirculation zone is generated by the horizontal motion of the impacting fluid and this zone allows for mixing of the fluid. This mixing helps regulate the temperature between the impacting fluid and the bulk fluid.

Heat transfer analysis is calculated in a similar way to normal convective heat transfer. Fluid dynamics are found in the manner just like flow within a pipe as the Reynolds number can be calculated from the nozzle diameter and the fluid velocity. The heat transfer rate can be calculated using Equation (2.13).

$$\dot{Q}_{conv} = hA_s(T_s - T_{jet}) \tag{2.13}$$

Coming back to the previously mentioned topic of nozzle-to-plate spacing. Lytle and Webb looked at the effects of low nozzle-to-plate spacings on the Nusselt number [22]. Using various distances and nozzle diameters they found that placing the nozzle closer to the surface created a great increase in the Nusselt number in a short distance from the stagnation point before dropping. Figure 2.7 shows the total results that they produced. What can also be noted from their results is the large increase in the convective heat transfer from the increase in Reynolds number. This shows that by increasing the rate at which flow is hitting the surface, the greater amount of heat transfer can occur. This makes sense since the jet is replacing fluid at a quicker rate keeping a lower temperature fluid in contact with the surface.

Other works have also looked into this topic, Choo et al. investigated the effects of nozzle-to-plate on the Nusselt number using a submerged impinging jet [23]. Using nozzle-to-plate spacings, ranging from 0.1 to 40, taken from various other research and their own experiments, they created an empirical correlation of the normalized stagnation Nusselt number based on the nozzle-to-plate spacings. Their correlation was compared to various

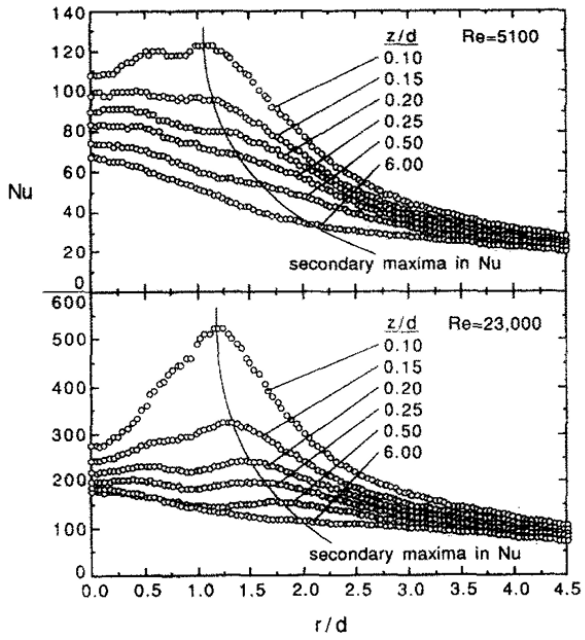

Figure 2.7: Variation of Nusselt number in the radial direction for various nozzle to plate spacings and two Reynolds numbers. [22]

experiments and was it was found that all experimental data fell within ±15% of the correlation. Their correlation can be seen in Equation (2.14).

$$Nu_0^* = \sqrt{4\exp^{-\left(\frac{H}{d}\right)/0.14} + \left\{0.57 - 0.5\tanh\left[\frac{\left(\frac{H}{d}\right) - 15}{11}\right]\right\}} \qquad (2.14)$$

Other research has been completed on this topic looking at other various effects other than the nozzle-to-plate spacing. Elison and Webb looked at the effect of different nozzle diameters and Reynolds number of the flow [24]. Figure 2.8 shows the results of their experiments, which determined that the nozzle diameter, nozzle-to-plate spacing, and the velocity at which the jet was impacting, all had positive effects on the Nusselt number.

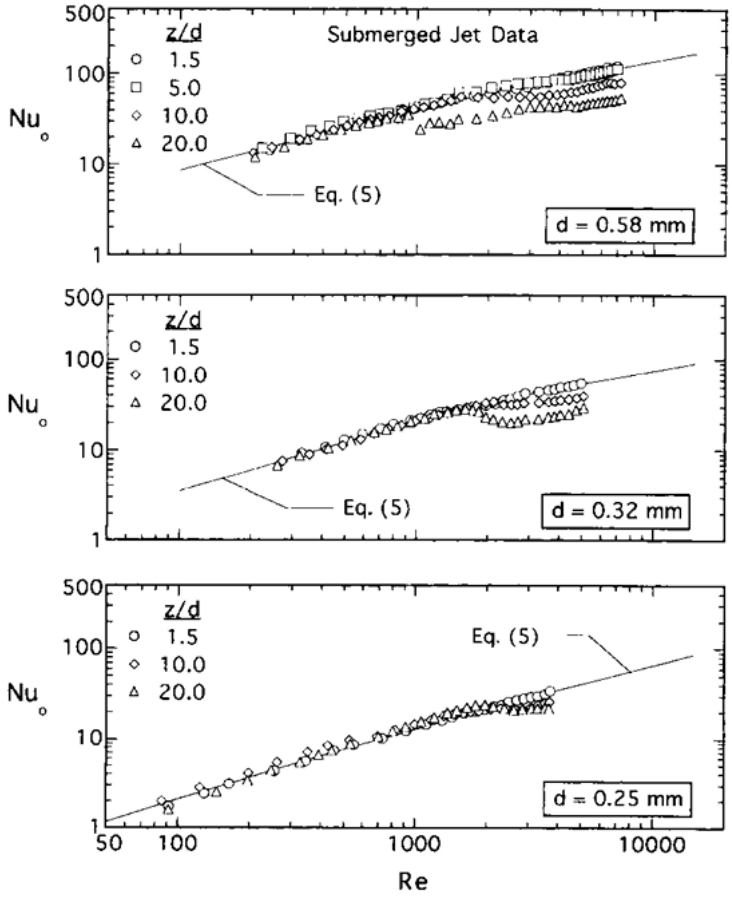

Figure 2.8: Variation of stagnation Nusselt number with Reynolds number for a submerged jet. [24]

2.4 - Two-Phase Flow

Two-phase flow is categorized by the presence of a flowing liquid and gas combination. It naturally occurs during boiling and other phase change phenomena but can also be implemented in impinging jets. The flow is commonly categorized by the volumetric

quality, which is the ratio of the amount of air over the total amount of water and air. The volumetric quality can be calculated using Equation (2.15). It can be seen from the equation that the volumetric quality, β, is the ratio of the volumetric flow rate of gas, Q_g, to the total volumetric flow rate of liquid (Q_l) and gas.

$$\beta = \frac{Q_g}{Q_g + Q_l} \tag{2.15}$$

Using Equation (2.15), the gas flow rate can be calculated from a set value of the liquid flow rate and a range of volumetric qualities. Equation (2.16) shows the equation used to determine the volumetric gas flow rates shown in Chapter 3.

$$Q_g = \frac{Q_l \beta}{(1 - \beta)} \tag{2.16}$$

Two-phase flow is also broken down into different flow regimes that occur based on the volumetric quality. The regimes are shown in Figure 2.9. The regimes are broken down into bubbly, slug, churn, annular and mist flow. Bubbly flow is when liquid dominates the flow pattern and small bubbles of gas flow throughout. Slug flow is when more gas is added and it combines into larger bubbles, but liquid still dominates the flow. Churn flow occurs when the volume of liquid and gas is similar so both phases are fighting for control of the flow. Annular flow is when gas takes over most of the volume, and a column of vapor occurs in the center of the flow, while the liquid sticks to the side of the

flow region due to surface tension and viscous effects. Mist flow is when gas dominates the flow and tiny droplets of liquid are suspended in the flow.

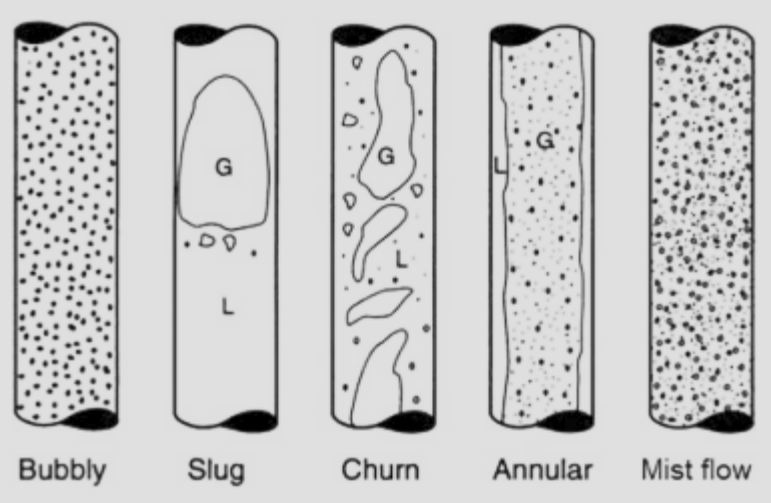

Figure 2.9: Schematic of the flow regimes of liquid-gas two-phase flow. [34]

Instead of gathering images of the flow, two-phase flow regimes can also be determined by the use of the volumetric flux, or the velocity of the different phases. Figure 2.10 shows the flow regimes based on the respective flux of each phase. This flux, j_p, can be found from the volumetric flow rate of the respective phase, Q_p, and the flow area, A_f. Equation (2.17) shows the formulation to calculate the volumetric flux.

$$j_p = \frac{Q_p}{A_f} \tag{2.17}$$

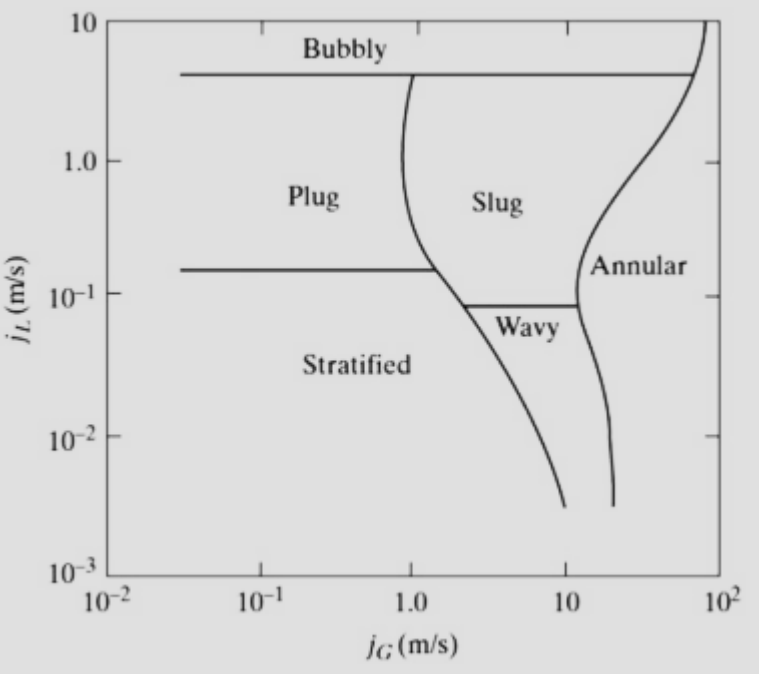

Figure 2.10: Mandhance-Gregory-Aziz's map for horizontal co-current gas-liquid flow. [34]

Two-phase flow is used outside of naturally occurring phenomena as a cooling method for various industries. It is commonly seen in steam generation as well as oil and gas applications. Research has been done on this topic with the use of two-phase mixtures in the application of flow boiling [25, 26] as well as with the use of impinging jets [27, 28, 29, 30]. Wu et al. looked at the heat transfer of a cylindrical surface subjected to an impinging jet at different nozzle-to-surface distances and low fluid velocities [31]. As seen in Figure 2.11, they found that the heat transfer rate increases slowly until the onset of nucleate boiling occurs and then it rises greatly until starting to reach the CHF and then it begins to slow again. They also saw that the system removed more heat as the velocity of

fluid was increased as well as when the distance between the nozzle and surface was increased. They determined that the increase in both jet velocity and nozzle to surface height have positive effects on the CHF.

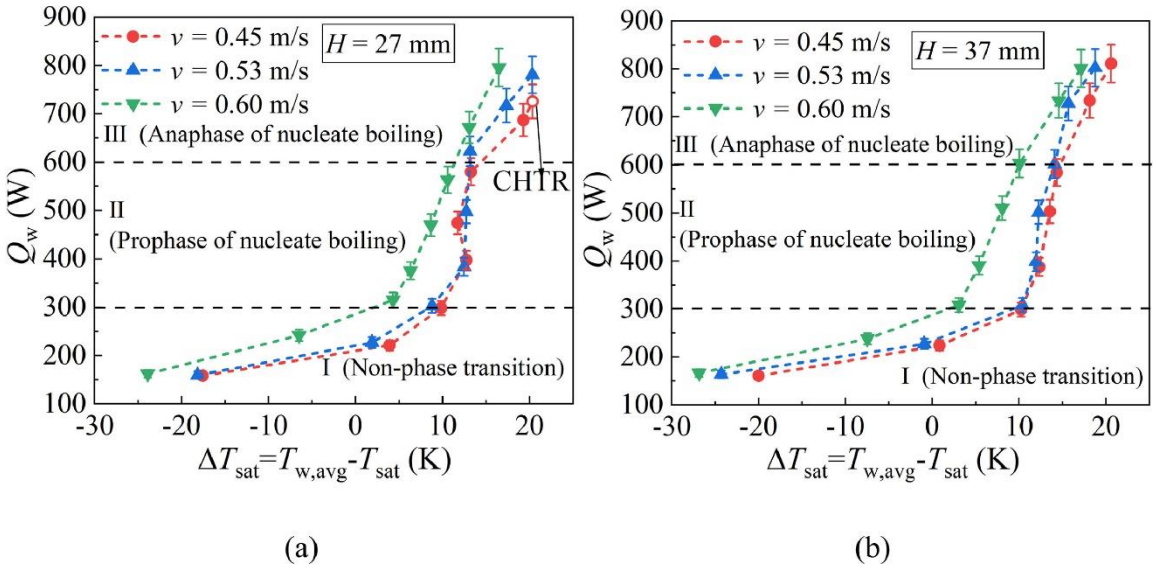

Figure 2.11: Boiling curves of impacting jet on cylindrical surface with different velocities, (a) H = 27 mm; (b) H = 37 mm. [31]

Piya et al. reviewed the effects of a submerged air-water jet on a plain surface using thermal imagery [32]. They used a system that had a vertical directed impinging jet that allowed the bubbles of air to naturally rise using buoyancy after being forced through the jet. They varied the air flow rate for values from $0.1 \leq \beta \leq 0.7$ using a Reynolds number of 24,000. With this setup, they discovered that the highest improvements in heat transfer occurred with a H/d = 4 with β = 0.3 and H/d = 2 with β = 0.2, each having a 47% increase in total heat transfer. They also observed that when the flow transitioned into the annular

regime a noticeable decrease occurred in the heat transfer. The total set of results can be seen in Figure 2.12.

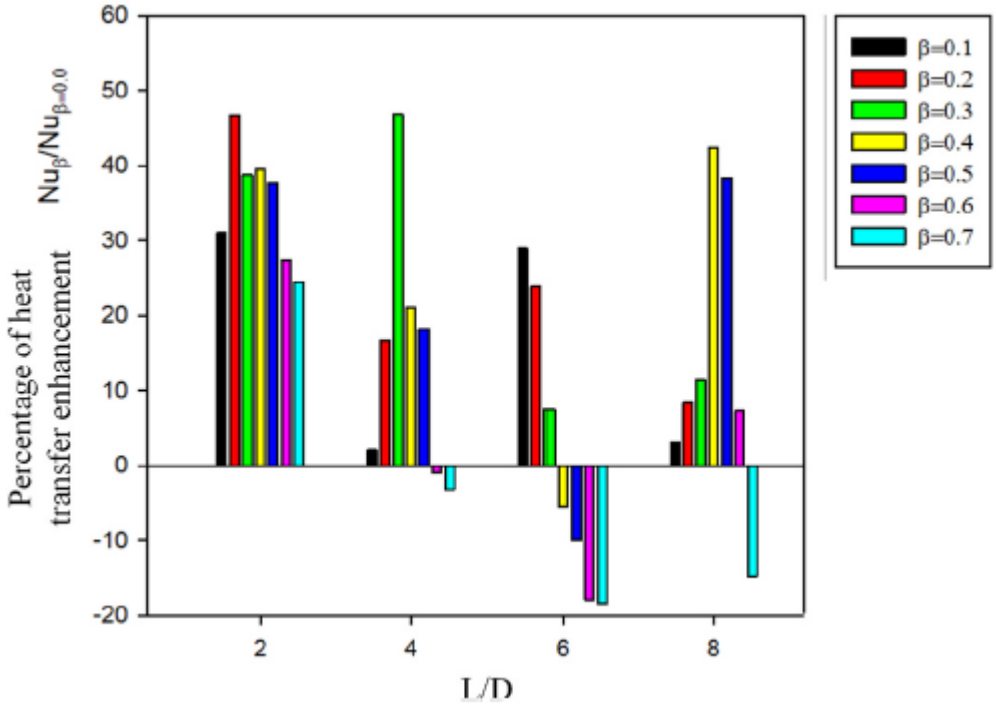

Figure 2.12: Comparison of the percent of heat transfer improvement compared to the average Nusselt number when β = 0.0. [32]

2.5 - Scope of Research

The goal of this research is to understand the effects of volumetric quality on the convective heat transfer coefficient of a porous surface subjected to two-phase jet impingement. The effects of fluid velocity and temperature were observed. The heat transfer coefficients were obtained at values of the volumetric quality ranging from 0 to 0.9 for both a plain and

porous surface. The surfaces were also placed in both a boiling and non-boiling scenario to compare the effect of changing volumetric quality. The bubble effect of the two-phase jet and the effect of changing the flow rate of fluid through the nozzle were explored. Based on the experimental results, the relationship between the volumetric quality and the convective heat transfer coefficient were obtained for both the plain and porous surface.

Chapter 3 - Experimental Setup

The experimental work done within this research was performed with the goal of combining the setups of a traditional pool boiling scenario with that of a two-phase submerged impinging jet. This setup allowed for the implication of testing at two different liquid-only Reynolds numbers of 732 and 2929 with nozzle-to-plate spacing of $H/d = 2$. The experiments were performed at volumetric qualities ranging from 0 to 0.9. This chapter will describe the apparatus and procedures of the experimental setup.

3.1 - Surface Types

Two surface types were tested within this experiment, a plain surface, and a columnar post wick porous surface. Copper was chosen as the material of both surfaces due to its high thermal conductivity and low specific heat. The plain surface was chosen since it was the most common surface seen in a pool boiling scenario. The actual surface used was the free surface of the heater apparatus which is shown later. The post wick was chosen due to its shrinking of the Rayleigh-Taylor instability wavelength, λ_{RT} leading to an improved CHF and its reduction of the wick thickness leading to a larger HTC. The post wick was also found to have the highest CHF compared to other porous surfaces as seen by Bevan [21].

3.1.1 - Plain Surface

The first surface type used was a plain surface. The surface had a size of a 13 mm (about 0.51 in) by 13 mm (about 0.51 in) square and was the exposed section of the heater

apparatus that is shown in Figure 3.4. This surface served as a base line when comparing to a porous surface due to its common use in boiling scenarios. The instability wavelength

$$\lambda_{ps} = \frac{9}{2\pi}\lambda_{RT}$$

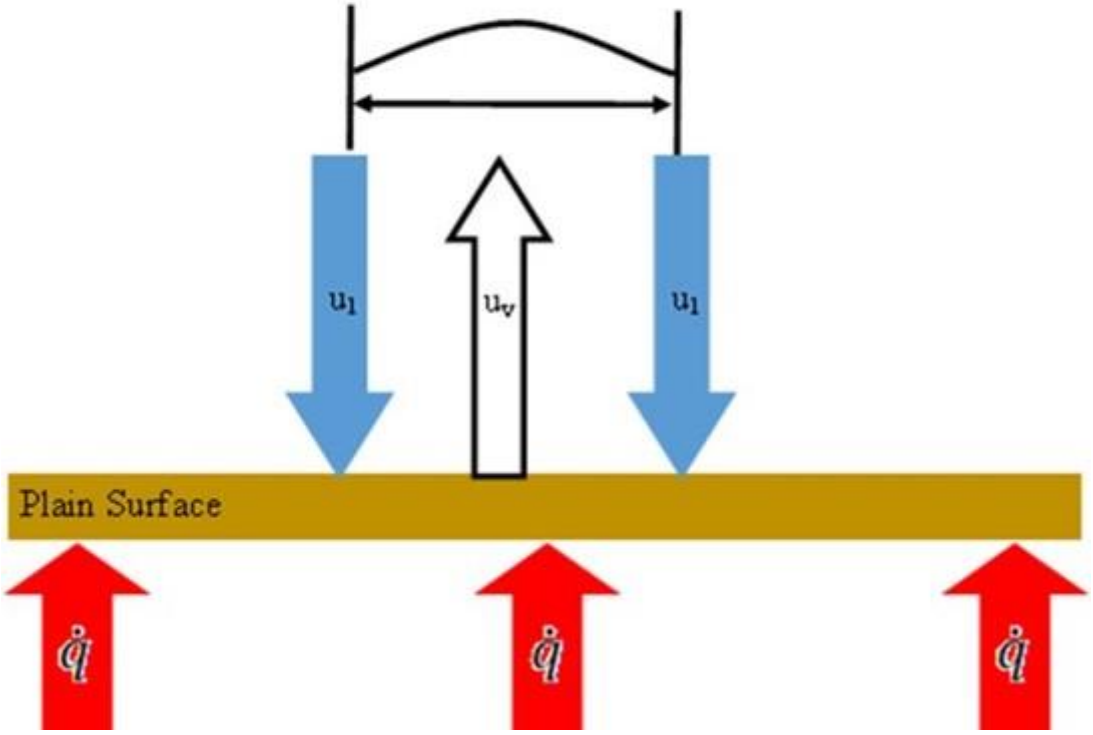

Figure 3.1: Schematic of a plain surface within a pool boiling scenario [21].

of the plain surface is the critical Rayleigh-Taylor wavelength and can be seen in Figure 3.1.

3.1.2 - Columnar Post Wick

The second surface used was a columnar post wick. This was the only porous surface used based on its performance in former research. The surface had a base size of 13 mm (about 0.51 in) by 13 mm (about 0.51 in) just like the plain surface and was manufactured using

copper-sintered particles with a diameter of 200 µm. The surface had 12 total posts with a diameter of 2.5 mm (about 0.1 in), a height of 2 mm (about 0.08 in), and a distance between

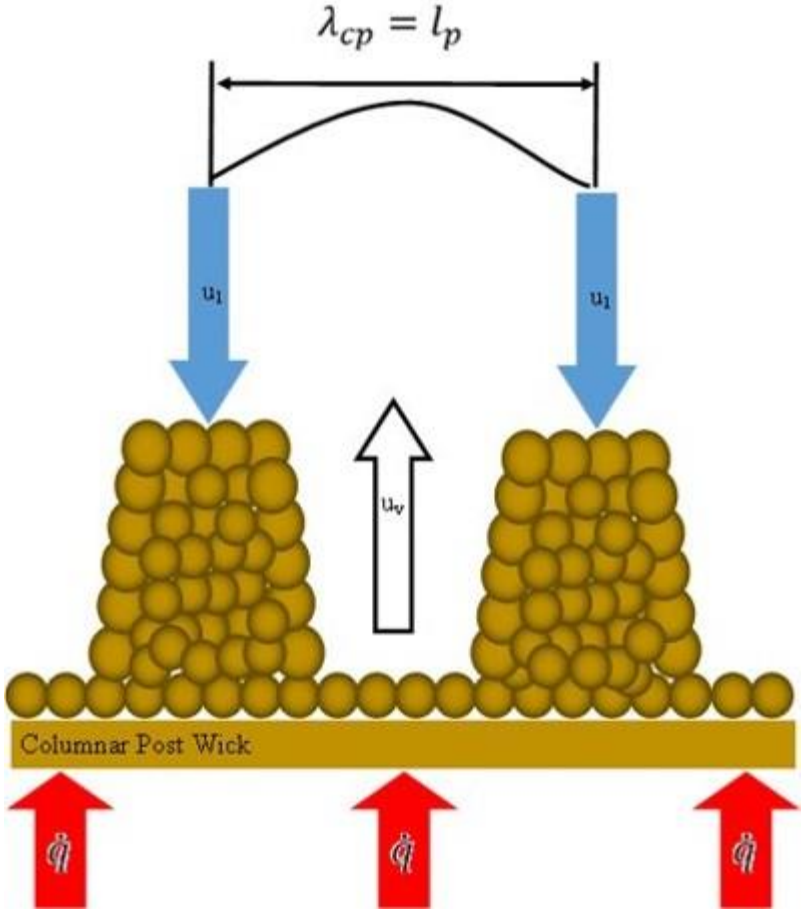

Figure 3.2: Schematic of a columnar post wick within a pool boiling scenario [21].

the posts (pitch distance, l_p) of 1 mm (about 0.04 in). This pitch distance dictates the Rayleigh-Taylor instability wavelength as seen in Figure 3.2 and microscopic images of the surface can be seen in figures Figure 3.3 and Figure 3.5.

3.2 - Heater Apparatus

The heater apparatus was the main component within this research. This setup allowed for the creation of an applied constant heat flux, the ability to collect temperature data, and

allowed for the transition to other surface types. Making up the heater is an internal copper block that allowed for the installation of six Tutco CH43810HW cartridge heaters. Two holes were placed 20 mm (about 0.79 in) apart that allowed for the placement of two K-type thermocouples that were used to determine the temperature of the impinging surface. Surrounding the heater is Teflon insulation that is needed to ensure heat loss is minimized during the experiment. Silicon sealant was used to ensure the system stayed watertight during the experiments and was placed in any open cracks. The surface types were attached to the impinging surface using solder to ensure a uniform connection that still allowed heat to transfer to the attached surface. The heater assembly can be seen in Figure 3.4 as well as a schematic in Figure 3.6. Not shown in the figure is the acrylic tube that was sealed to the top surface of the heater to create a pool for a submerged impinging jet but can be seen in the schematic within Figure 3.6.

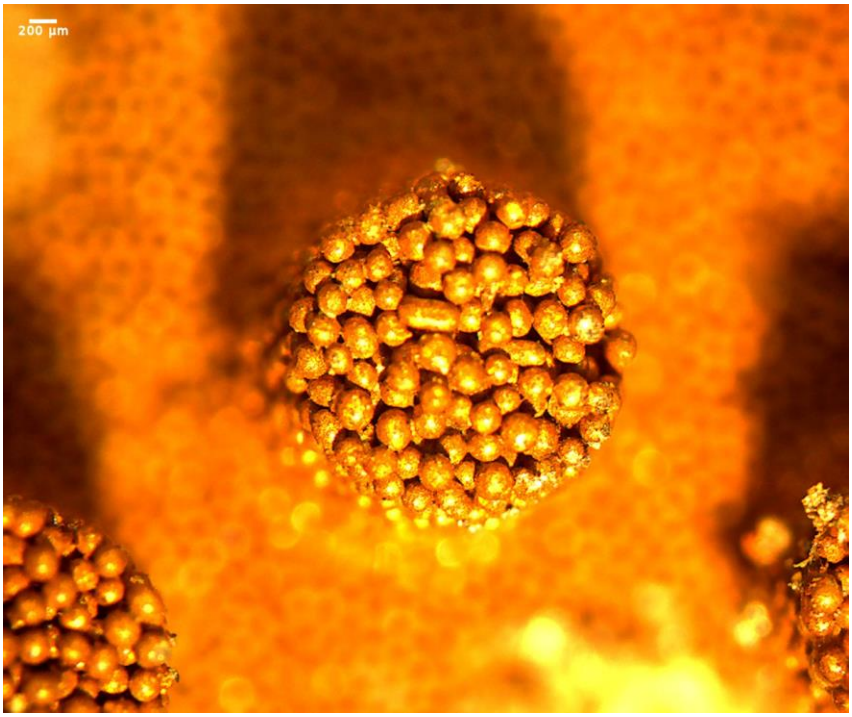

Figure 3.3: Microscopic image showing particle and post sizes.

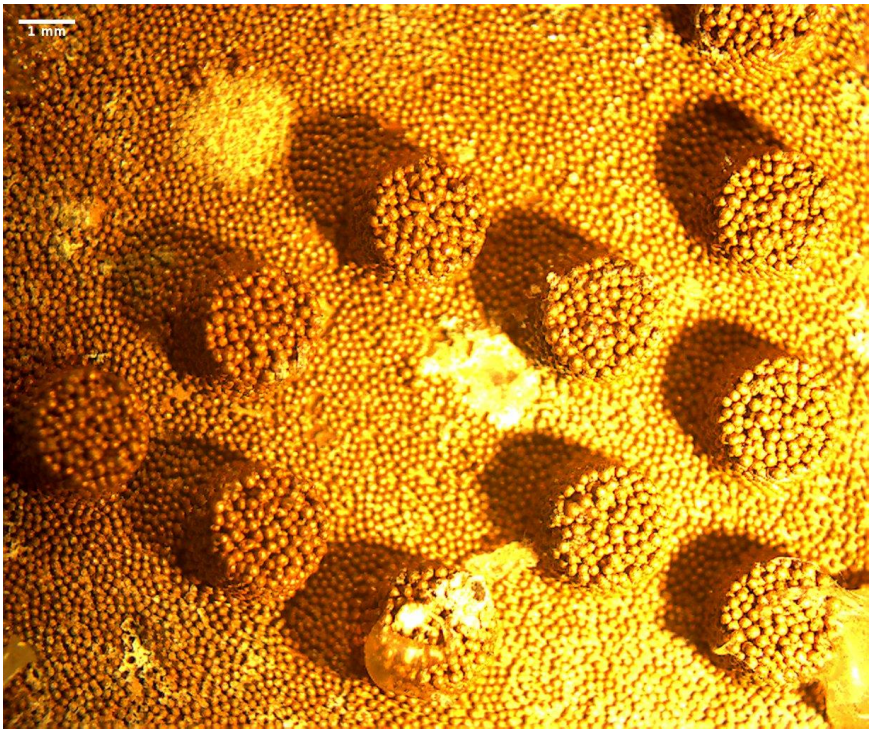

Figure 3.5: Microscopic image showing the posts and the distance

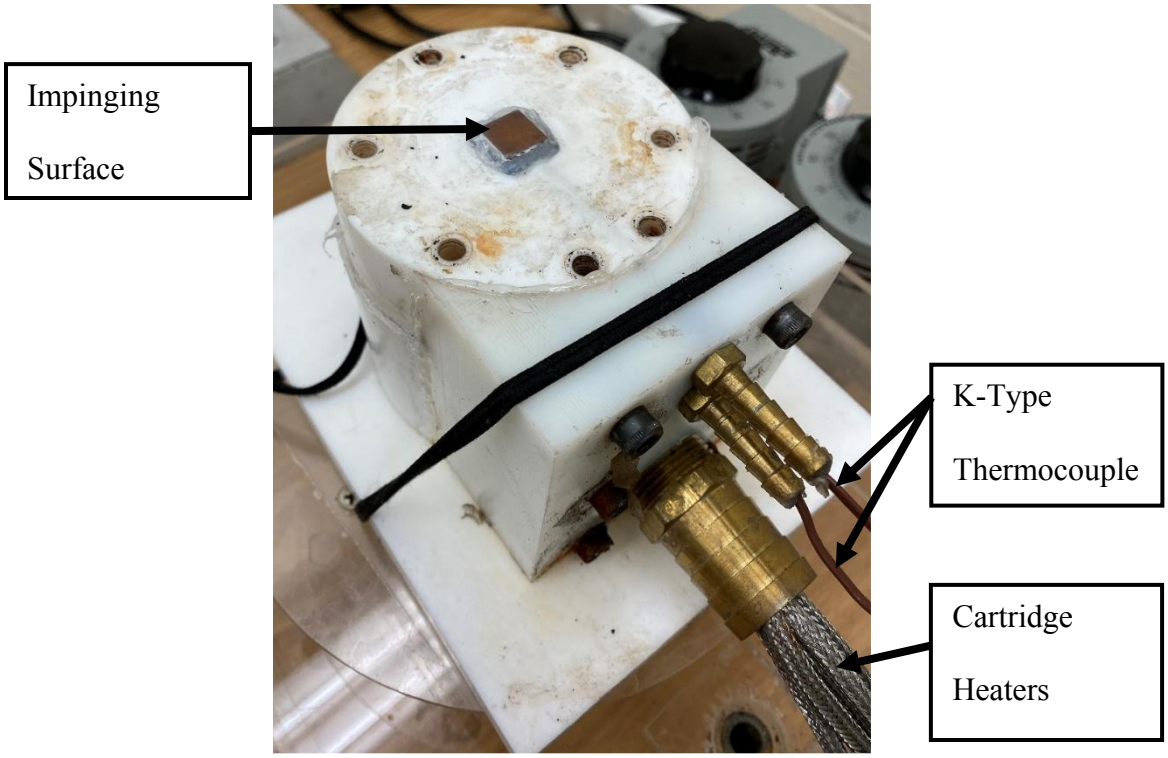

Figure 3.4: Heater apparatus with the plain impinging surface and showing key components.

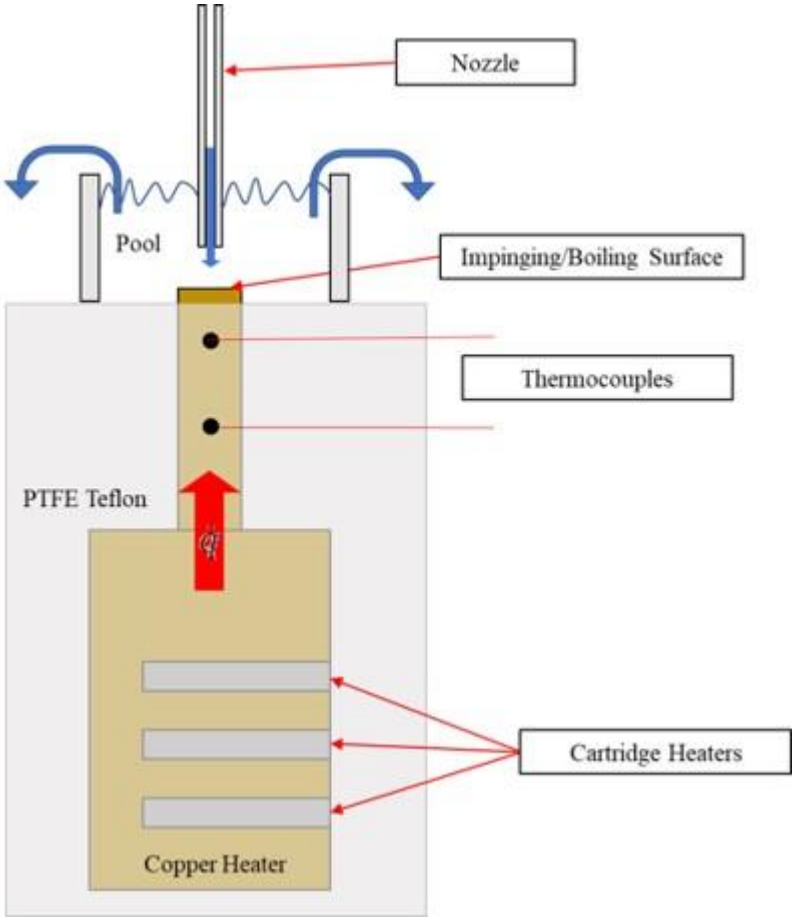

Figure 3.6: Cross section schematic of the heater showing internal parts as well as the attached pool location [21].

Two variable transformers were used to control the cartridge heaters. The transformers used were the Staco Energy 3PN10101B. These transformers allowed for a variable output voltage of 0-140V at 10 A. With these, the applied heat flux to the impinging surface was able to be controlled using the voltage and could be held at a constant heat flux. Three heaters were connected in parallel to each transformer to allow ease of control. Figure 3.7 shows the transformers used with the heater.

Figure 3.7: Staco Energy transformers used to power the cartridge heaters.

Temperature was captured in real time using the two K-type thermocouples connected to a data recorder. The recorder used was an Omega OM-CP-QuadTemp2000 and allowed for the collection of up to four different temperature inputs. This recorder was then connected to a laptop that allowed for real time visual of the temperature values using their software. This software made the collection of data simple and for quick export to Excel for post-processing.

3.3 - Flow Apparatus

The flow apparatus had to be able to encompass the submerged impinging jet in both non-boiling and boiling scenarios, while also implementing the two-phase mixture. The components included the temperature bath, water flow meters, the nozzle with a stage for height adjustment, and air flow meters. The temperature bath used, shown in Figure 3.8, was the Polystat AD07H200. This bath allowed for the setting of the water temperature, with a range of 10-200°C, that could be adjusted between boiling and non-boiling tests that will be discussed later. The bath also served as the pump for the system. All components in the setup were connected using flexible tubing that varied in diameters. The water flow

meters used were from Dwyer, seen in Figure 3.9. These flow meters had ranges of 10-100 cc/min and 0-0.75 l/min, which allowed for the setting of two different flow rates to be tested in each experiment. The nozzle and stage, depicted in Figure 3.12, consisted of a stainless steel IDEX nozzle that had an inner diameter of 2 mm (about 0.08 in). This size nozzle allowed for adequate water flow while allowing smaller bubbles to be formed at

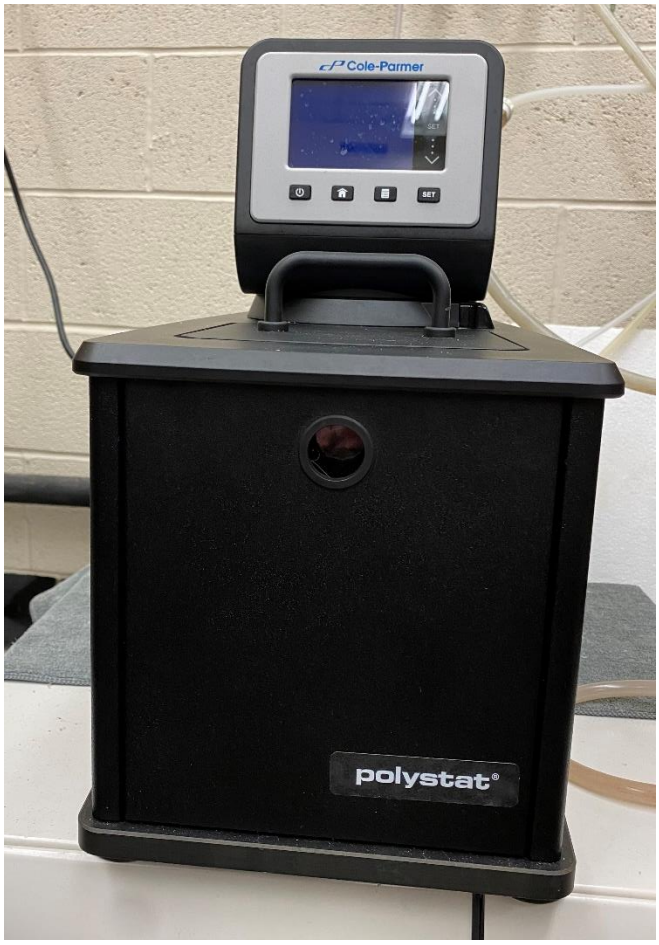

Figure 3.8: Polystat temperature bath used throughout the experiment.

lower volumetric qualities, instead of larger bubbles that were present in smaller nozzles. The nozzle was connected to an adjustable stage that could be used to set the nozzle to plate spacing using the attached micrometer. The air flow meters, shown in Figure 3.10, had ranges of 10-100 cc/min and 100-1000 cc/min and were tubed together to allow for

easy transition between the two. This transition needed to be done to encompass all the flow rates that were calculated based on the volumetric quality value. During a test one valve would be shut and the other would be opened to switch between the two flow ranges. Figure 3.11 shows the schematic of the combination of the flow and heater apparatuses.

(a) *(b)*

Figure 3.9: (a) Dwyer 10-100 cc/min water flow meter (b) Dwyer 0-0.75 l/min water flow meter

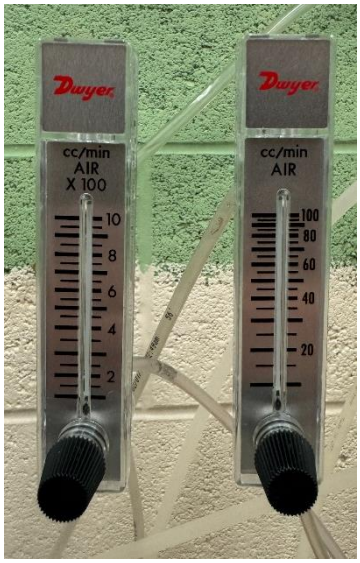

Figure 3.10: Air flow rate meters used to test all volumetric qualities.

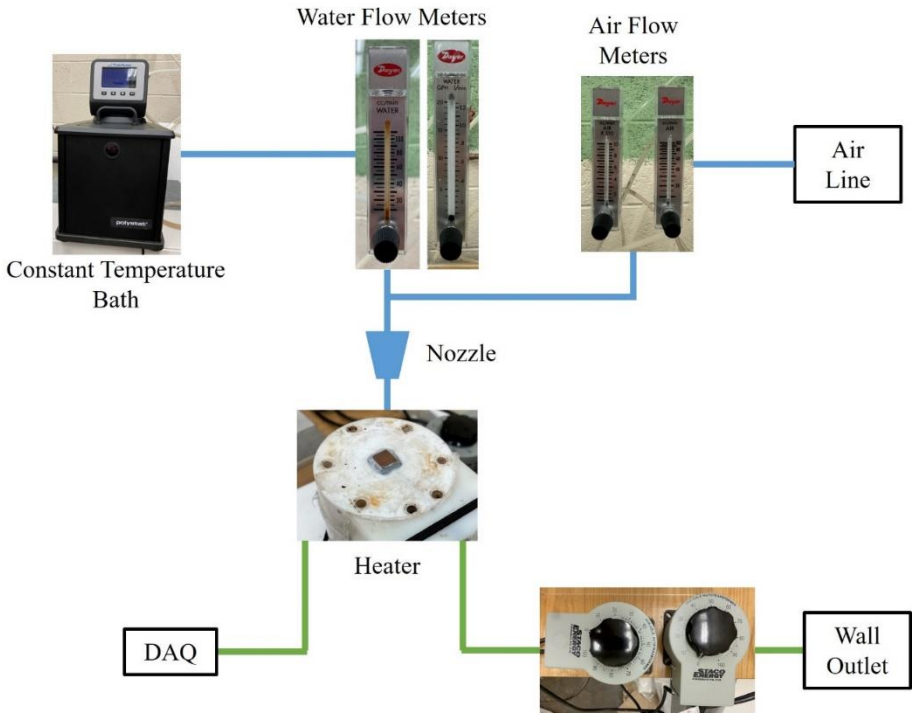

Figure 3.11: Schematic of the entire apparatus setup.

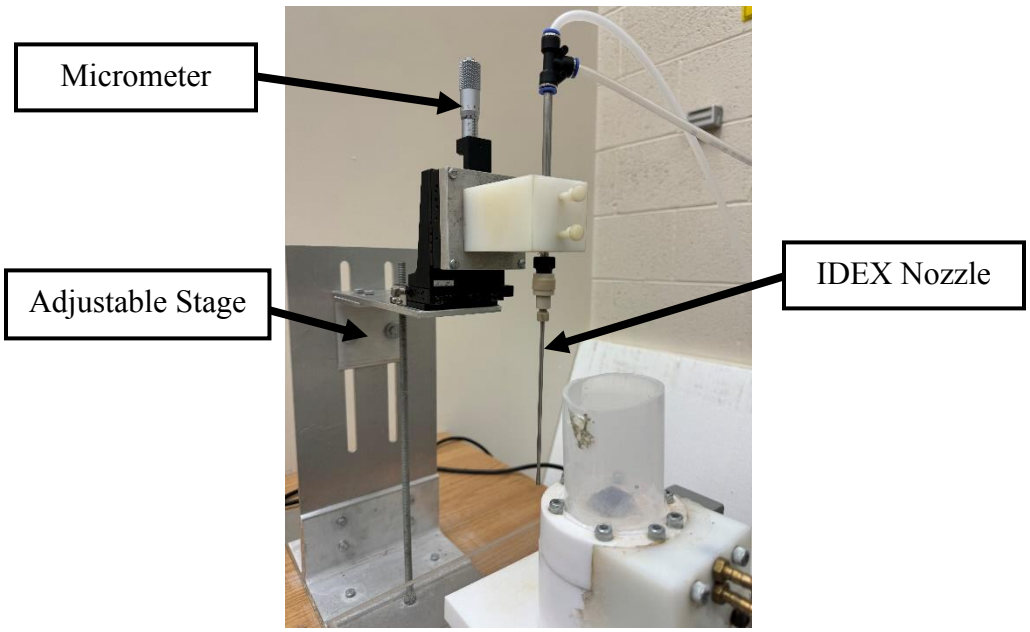

Figure 3.12: Adjustable stage with nozzle

3.4 - Procedure

To begin the experiments, the flow rates of water needed to be chosen and the flow rates of the air needed to be calculated from those values. Two water flow rates were chosen, 50 and 200 cc/min. These values represent the Reynolds numbers of 732 and 2929, respectively. It can be seen from these Reynolds values that one is laminar, and one was transitional. This was not chosen on purpose but did serve as another way to compare the two flow rates.

With these water flow rates, their respective air flow rates could be chosen based on volumetric quality, β values ranging from 0-0.9. Table 3-1 shows the determined air flow rate values that were used throughout this experiment. These flow values were used in both the non-boiling and boiling scenarios. It can be seen from Table 3-1 that no test could be performed on the surfaces with a water flow rate of 200 cc/min and a volumetric quality of 0.9. This was due to the air flow meters used not having the range to cover that high of a flow rate, so it was ignored during the testing.

Table 3-1: Air flow rate values in cc/min based on desired water flow rates.

Water Flow Rate [cc/min]	**Volumetric Quality, β**								
	0.1	**0.2**	**0.3**	**0.4**	**0.5**	**0.6**	**0.7**	**0.8**	**0.9**
50	5.55	12.5	21.43	33.33	50	75	116.67	200	450
200	22.22	50	85.71	133.33	200	300	466.67	800	-

With the flow rates determined the actual experimental procedure can be discussed. The procedure started with ensuring the nozzle-to-plate spacing, *H/d*, was set to two before each test. This value was set using the aforementioned stage. This was completed by placing the end outlet of the nozzle on the impinging surface and then using the attached micrometer on the stage to set the desired distance, which in this case was 4mm (about 0.16 in). Once this distance was set, all tubing was connected, and the water supply/heating bath was turned on. In the non-boiling case, the water temperature was set to a value of 35°C, and 90°C for the boiling case. These values ensured that, with the constant applied heat flux, the water leaving the nozzle would not affect the non-boiling or boiling conditions. The desired water flow rate was then set based on which flow meter was required. Once the recorded temperature had reached a steady temperature, ± 1°C, for an interval of 3 minutes, the test was started. Temperatures were then collected for each volumetric quality value until all air flow rates were complete, with flow rates not being changed until the previous conditions were met. As mentioned in the apparatus, when the air flow rate values exceeded the values on one flow meter, the valve was shut on one and the other valve was opened to meet the desired flow rate. This was repeated twice for each water flow rate and for each non-boiling or boiling scenario, for eight tests per test surface. Once all data was collected for a given surface type, the previous steps were repeated for the other surface.

Chapter 4 - Results and Discussion

4.1 - Flow Regime

To get confirmation on the different types of two-phase flow that were being applied to the system, the liquid and gas volumetric fluxes were calculated. This method of determining the flow regimes was discussed in Chapter 2 and Figure 2.10 is a similar plot to what is shown in Figure 4.1.

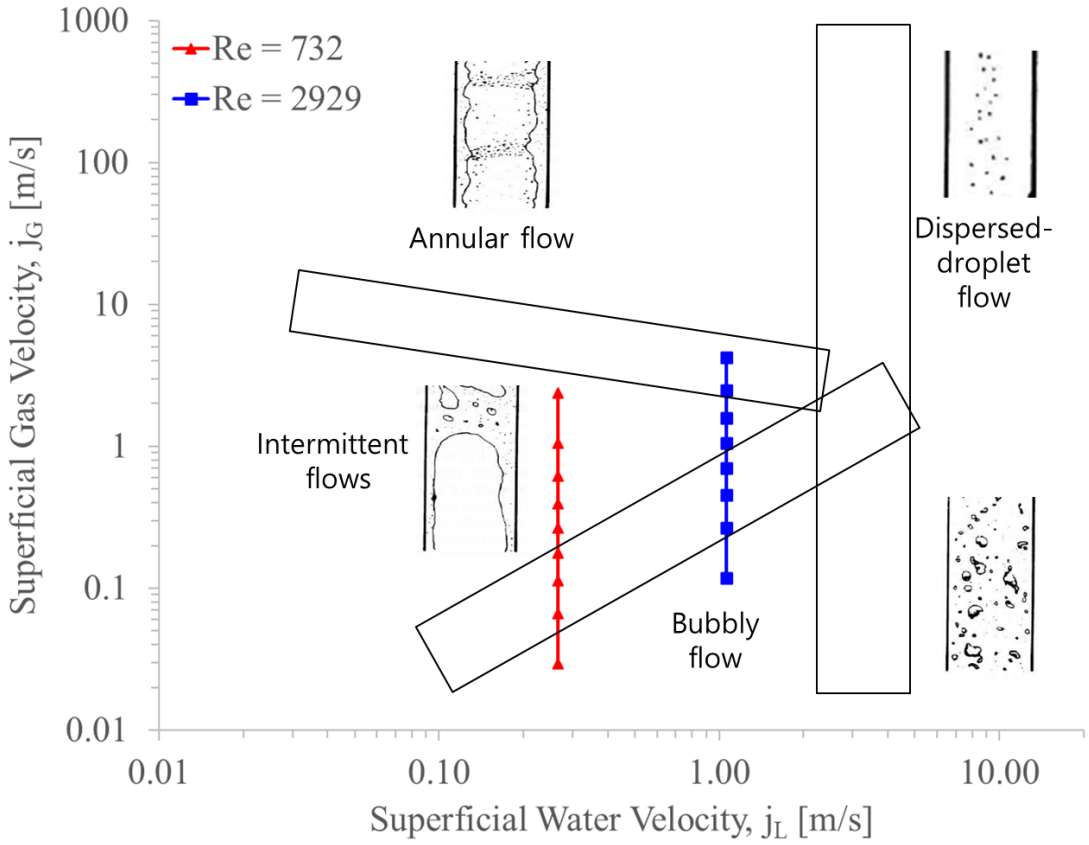

Figure 4.1: Two-phase flow regimes from this experiment based on the volumetric fluxes.

From Figure 4.1, it can be noticed that due to the low Reynolds number of the water flow rate, the flow regimes only consist of bubbly and intermittent flows. These types of flows are expected to achieve the best heat transfer as has been seen in previous work.

Two water flow rates were chosen that represented Reynolds numbers of 732 and 2929. Table 4-1 shows the water flow rates and the corresponding Reynolds number. The values for the air flow rates based on volumetric quality and water flow rates can be seen in Table 3-1. As can be seen from the Reynolds numbers, one of the flow rates is laminar and the other in the transitional region. This allowed for the comparison between the separate regimes. Since the water flow rate was held constant throughout the experiment, all data is broken up based on these two Reynolds numbers and the respective surface type that was being tested.

Table 4-1: Water flow rates and their respective Reynolds number values.

Water Flow Rate [cc/min]	**Reynolds Number**
50	732
200	2929

Photos of the two-phase mixture leaving the nozzle were also taken for each of the tests. This was done to depict the amount of bubble generation as an increase in the volumetric quality occurred. Figure 4.3 through Figure 4.8 show all the photos based on surface type, scenario, and Reynolds number for three distinct volumetric quality values.

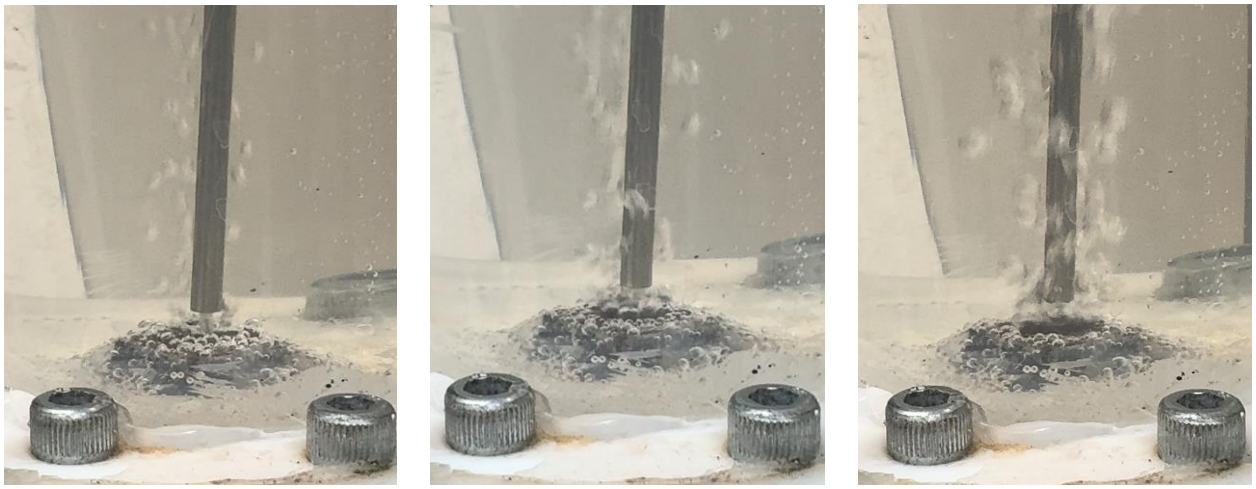

β = 0.2 β = 0.5 β = 0.8

Figure 4.3: Bubble visualization of the plain surface in non-boiling conditions and Re = 732.

β = 0.2 β = 0.5 β = 0.8

Figure 4.2: Bubble visualization of the plain surface in non-boiling conditions and Re = 2929.

β = 0.2 β = 0.5 β = 0.8

Figure 4.5: Bubble visualization of the post-wick surface in non-boiling conditions and Re = 732.

β = 0.2 β = 0.5 β = 0.8

Figure 4.4: Bubble visualization of the post-wick surface in non-boiling conditions and Re = 2929.

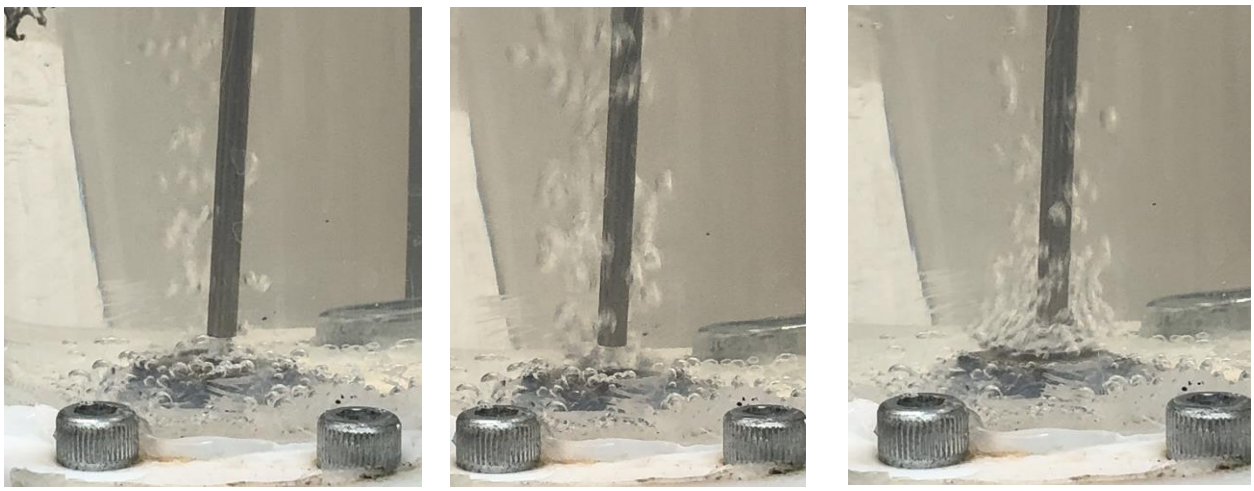

β = 0.2 β = 0.5 β = 0.8

Figure 4.7: Bubble visualization of the plain surface in boiling conditions and Re = 732.

β = 0.2 β = 0.5 β = 0.8

Figure 4.6: Bubble visualization of the plain surface in boiling conditions and Re = 2929.

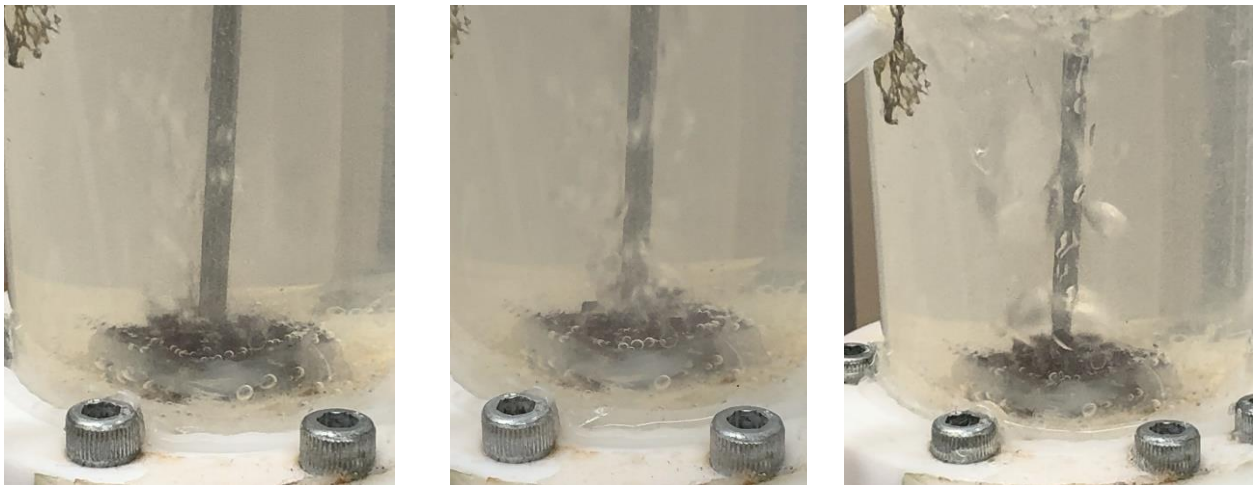

β = 0.2 β = 0.5 β = 0.8

Figure 4.9: Bubble visualization of the post-wick surface in boiling conditions and Re = 732.

β = 0.2 β = 0.5 β = 0.8

Figure 4.8: Bubble visualization of the post-wick surface in boiling conditions and Re = 2929.

4.2 - Non-Boiling Experiment

The non-boiling experiment was performed to act as a baseline for the improvement that is seen during the boiling experiment. The results are shown as a correlation between the HTC and the volumetric quality. Figure 4.10 shows the difference between the two surfaces at Re = 732 for volumetric qualities of $0 \leq \beta \leq 0.9$. From this figure it can be seen that the HTC slightly varies at lower qualities but then starts to increase before reaching a maximum HTC of 5062 at β = 0.8 for the plain surface. The overlapping of the two graphs is most likely due to the low water flow rate. Similarly for the post-wick, the HTC starts to increase at higher qualities before reaching a maximum HTC of 7293 at β = 0.9. Figure 4.11 shows the same two surfaces and attributes but at Re = 2929. With the increase in Reynolds number the benefit of the post-wick surface can be seen as the difference in the

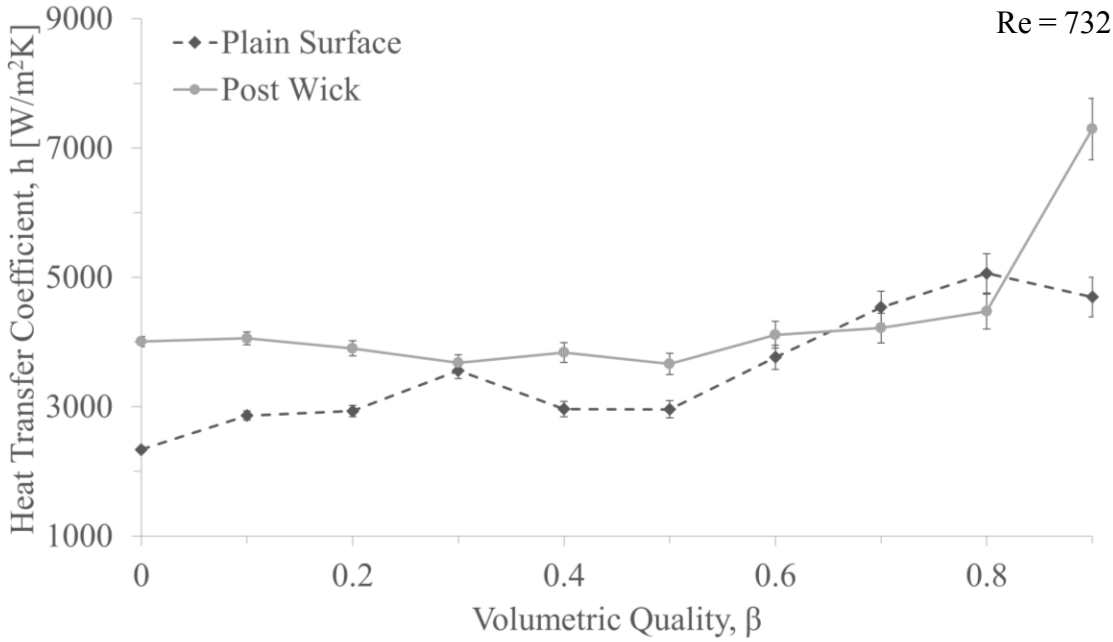

Figure 4.10: Non-boiling HTC vs volumetric quality at Re = 732 for each surface.

HTC compared to the plain surface is around 5000. From these figures it can be concluded that the added air to the impinging jet has a positive effect on the total heat transfer system and is best shown at higher flow rates of air since the system becomes more turbulent.

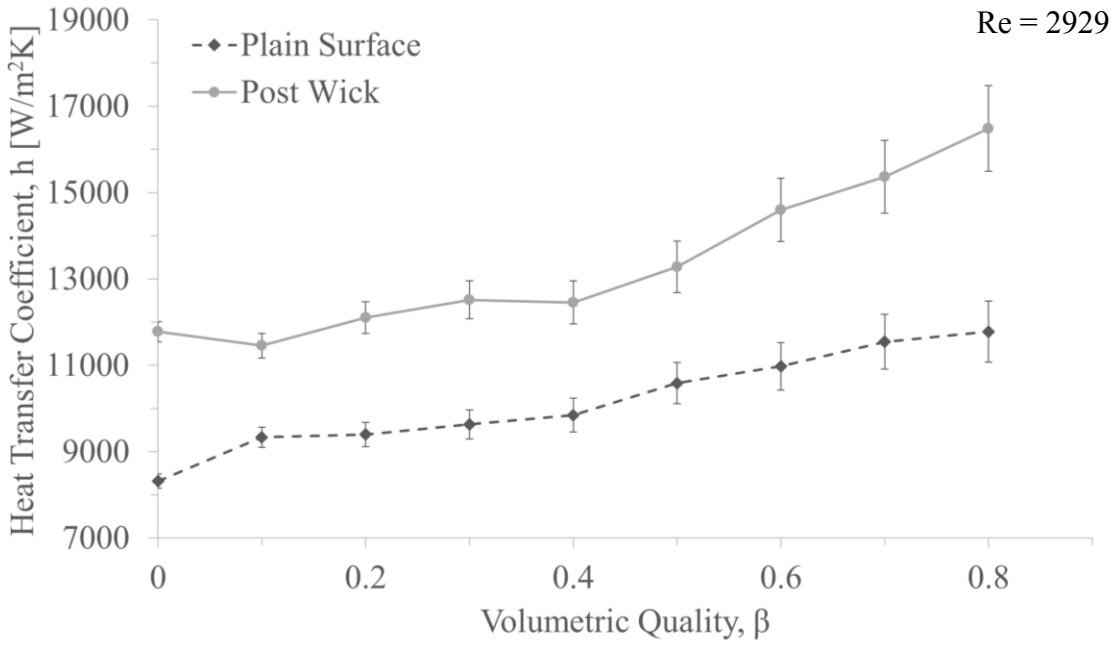

Figure 4.11: Non-boiling HTC vs volumetric quality at Re = 2929 for each surface

A comparison was also made between the different Reynolds number on each surface. These can be seen in Figure 4.13 and Figure 4.12. On both surfaces, it can be seen that the increase in the Reynolds number causes about a 4x increase in the HTC with a single-phase jet. With the plain surface, this difference drops to around 3x at higher volumetric qualities. As for the post-wick, the increase in volumetric quality didn't show any effect on the HTC at a low Reynolds but shows a large effect at the higher Reynolds. This likely due to the increased replacement rate of liquid to the heater surface.

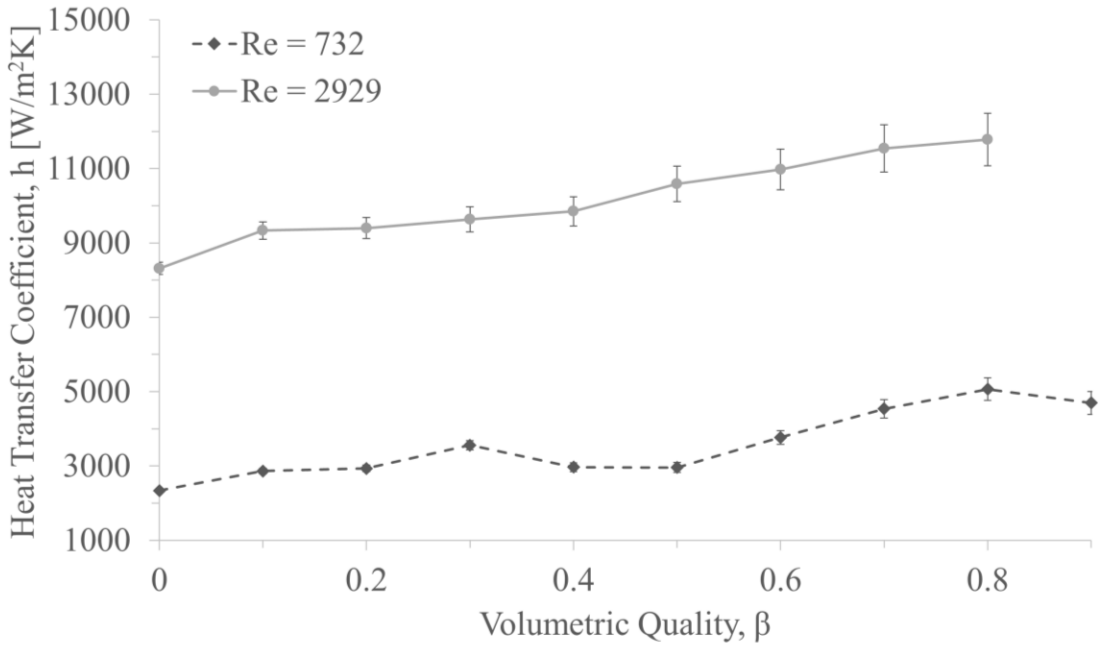

Figure 4.13: Non-boiling HTC vs volumetric quality of the plain surface at different Reynolds number.

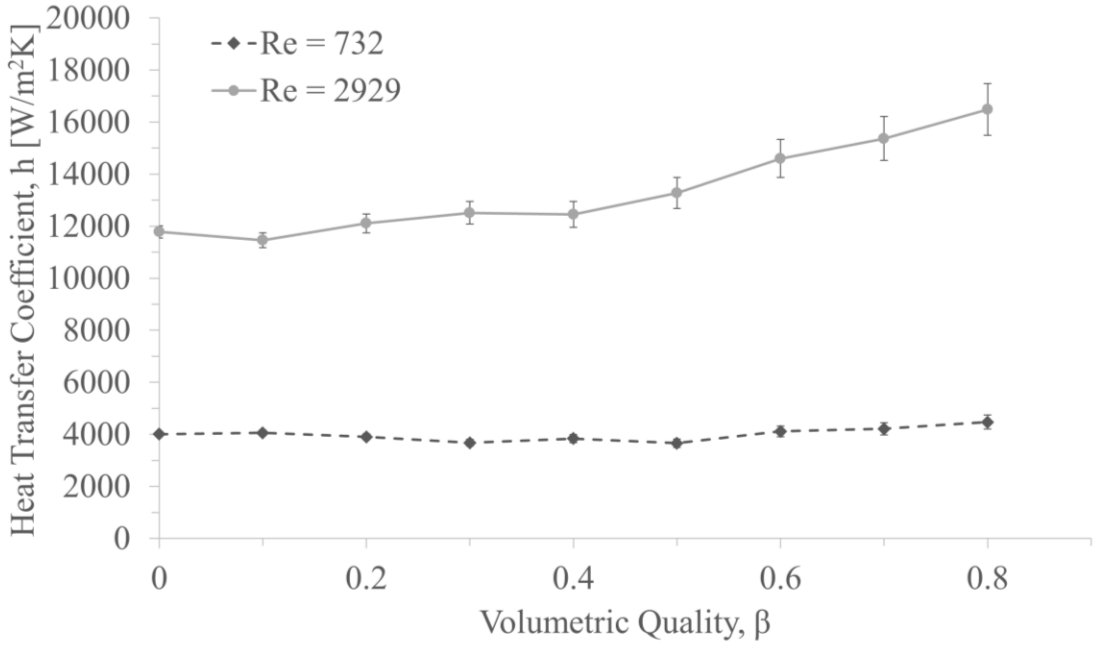

Figure 4.12: Non-boiling HTC vs volumetric quality of the post-wick surface at different Reynolds number.

4.3 - Boiling Experiment

The goal of the boiling experiment was to see if the added bubble effect of the two-phase nozzle had as large of an effect on the HTC compared to the non-boiling experiment. This was done by heating both the plain and post-wick surface to a temperature above the saturation point of water. Both surfaces were analyzed to make a comparison between a plain and porous surface.

4.3.1 - Validation

Validation of the boiling setup had to be completed before collecting data to ensure accurate results. This was done by testing the setup in a pool boiling scenario without an added porous surface or impinging jet. The plain surface was used and was compared against the correlation that Rohsenow [7, 8, 9] created. Equation (4.1) shows the correlation. One of the key parameters in the correlation is that of the heater surface. Hence, the Rohsenow correlation only applies to a clean and polished surface. This was why the plain surface was used for the validation as it is the only that follows these conditions.

$$\dot{q}_{nucleate} = \mu_l h_{fg} \left[\frac{g(\rho_l - \rho_v)}{\sigma}\right]^{\frac{1}{2}} \left[\frac{c_{pl}(T_s - T_{sat})}{C_{sf} h_{fg} Pr_l^n}\right]^3 \qquad (4.1)$$

Figure 4.14 shows the Rohsenow correlation plotted with the present study. The correlation was plotted with ±20% uncertainty to all for experimental error in the setup of

the present study. Error bars are included on the data of the present study showing an error of 5% due to the measurements of the surface temperatures to calculate ΔT_{excess}. This validation shows the validity of the experimental setup and allows for the continuation to the comparison of the two surface types.

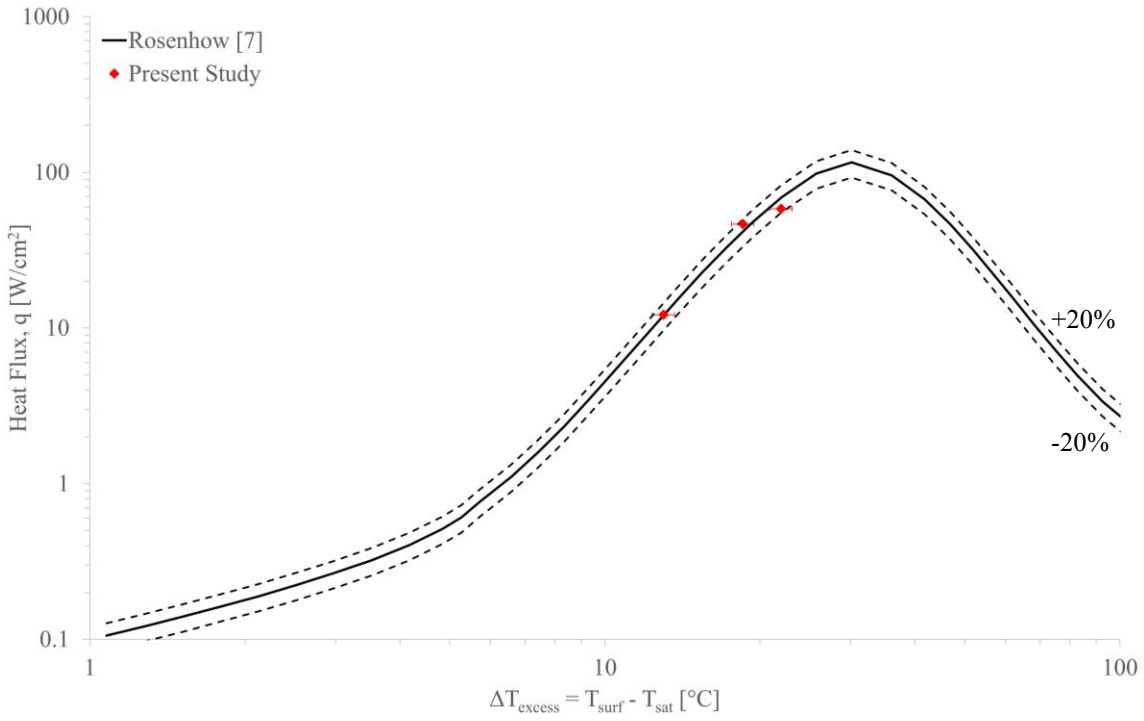

Figure 4.14: Validation of experimental boiling setup.

4.3.2 - Results

As previously mentioned, the boiling results had a total of two flow rates and values of the volumetric quality from $0 \leq \beta \leq 0.9$. The volumetric quality of 0 represented the effects of a single-phase impinging jet and allowed for a baseline when comparing to a two-phase jet. A comparison was made between the two surfaces using the HTC and the change in volumetric quality. Figure 4.15 and Figure 4.16 show this comparison.

Looking at Figure 4.15, it can be seen that the post-wick vastly outperforms the plain surface, which is expected. With the added monolayer surface and the controllable hydrodynamic wavelength from the posts, the post-wick at Re = 732, achieved a HTC of 32742 at β = 0.9. This performance of the post-wick can also be seen at the higher Reynolds. The post-wick achieved its highest HTC at β = 0.7 with a value of 34260. It should be noted that in each figure, the increase that is seen from the added bubble effect is within the margin of error. Due to this margin, it can be concluded that the added air to the impinging jet has a minimal to negligible effect on the total heat transfer of the system. Boiling dominates the heat transfer, while the water from the impinging jet adds some to the system and air has little effects. This is true for both the surfaces as both trends show little effect caused by the air. This air effect is noticeable in the non-boiling experiment but lacks to show when boiling.

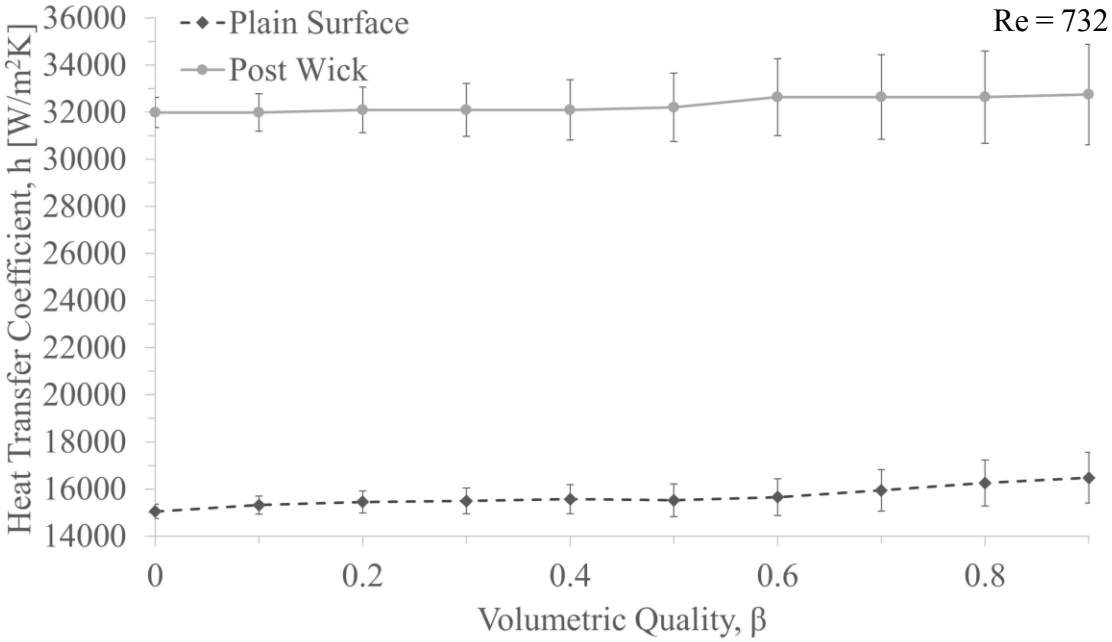

Figure 4.15: Boiling HTC vs volumetric quality at Re = 732 for each surface.

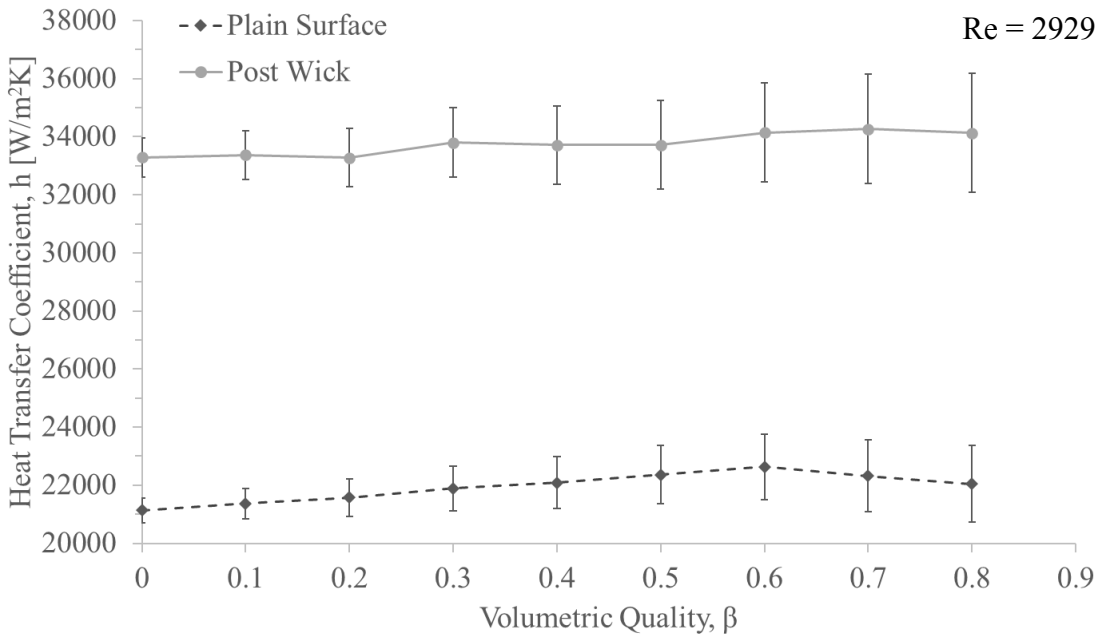

Figure 4.16: Boiling HTC vs volumetric quality at Re = 2929 for each surface.

Just like the non-boiling experiment, a comparison was made between the two different Reynolds numbers for the boiling experiment. Figure 4.17 shows this comparison. With the plain surface in a boiling scenario the change in Reynolds numbers had less of an effect on the HTC compared to the non-boiling experiment by only having approixamte 1.5 times increase. A comparison was also made between the single-phase jet, volumetric quality of 0, and the highest HTC achieved in each experimental case. These comparisons can be seen in Table 4-2 as well as Figure 4.18 and Figure 4.19. The curves in Figure 4.18 and Figure 4.19 were created using the nomralized HTC at each volumetric quality when compared to single-phase impinging jet. The normalized

HTC, h^*, was created using Equation (4.2), where h_β, is the HTC at a given volumetric quality and $h_{\beta=0}$, is the HTC at a volumetric quality of 0 or a single-phase jet.

$$h^* = \frac{h_\beta}{h_{\beta=0}} \tag{4.2}$$

From Figure 4.18 and Figure 4.19, it can be seen that the effects of the added two-phase jet is more noticable in the non-boiling cases. This is due to boiling dominating the heat transfer of the overall system. It should be noted that the results of the boiling experiment show that the added air to the impinging jet has a larger effect on the plain surface when compared to that of the post-wick. This is mostly due to the geometry of the post-wick being more equipt to boiling rather then the impacting bubbles. One thing to notice about the post-wick is its performance at a lower Reynolds number in the boiling scenario. In this scenario nucleation sites occur on the post-wicks but do not release from the surface in locations further away from the stagnation zone. This is due to the posts disrupting the impacting fluid and not disturbing the formed bubbles that create insulation areas. This is what creates the decreasing performance of this surface. It can be seen that once more air is added to the impinging jet, enough of the bubbles are disturbed to increase the heat transfer.

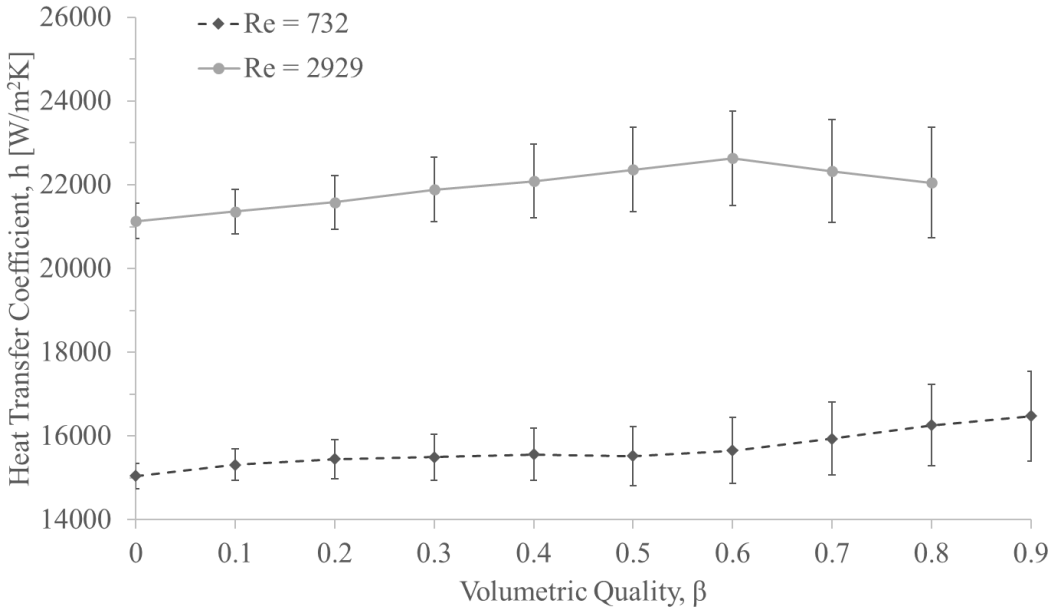

Figure 4.17: Boiling HTC vs volumetric quality of the plain surface at different Reynolds number.

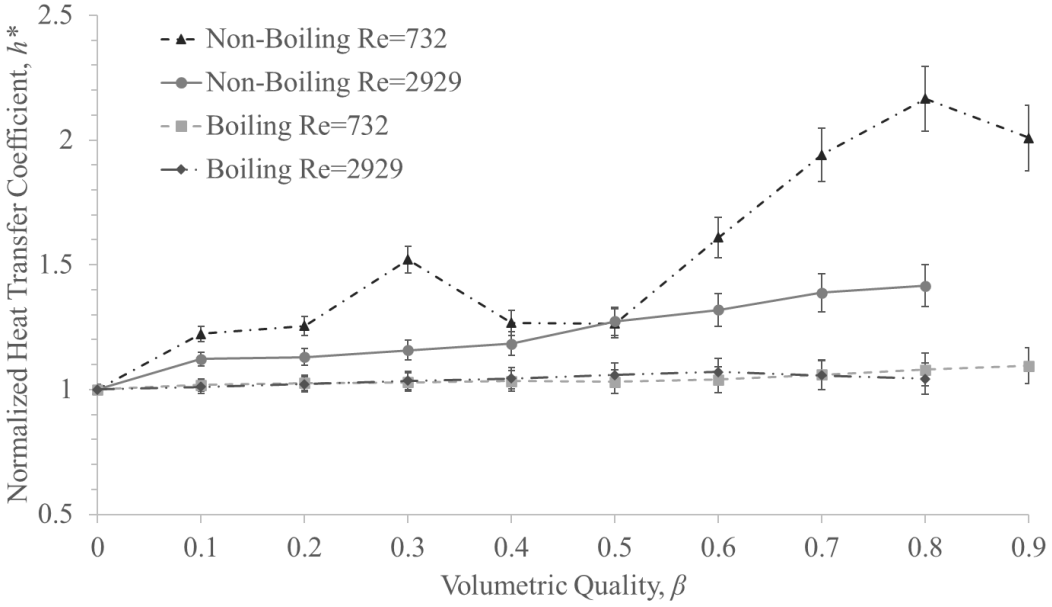

Figure 4.18: Normalized HTC showing the effect of volumetric quality on the plain surface.

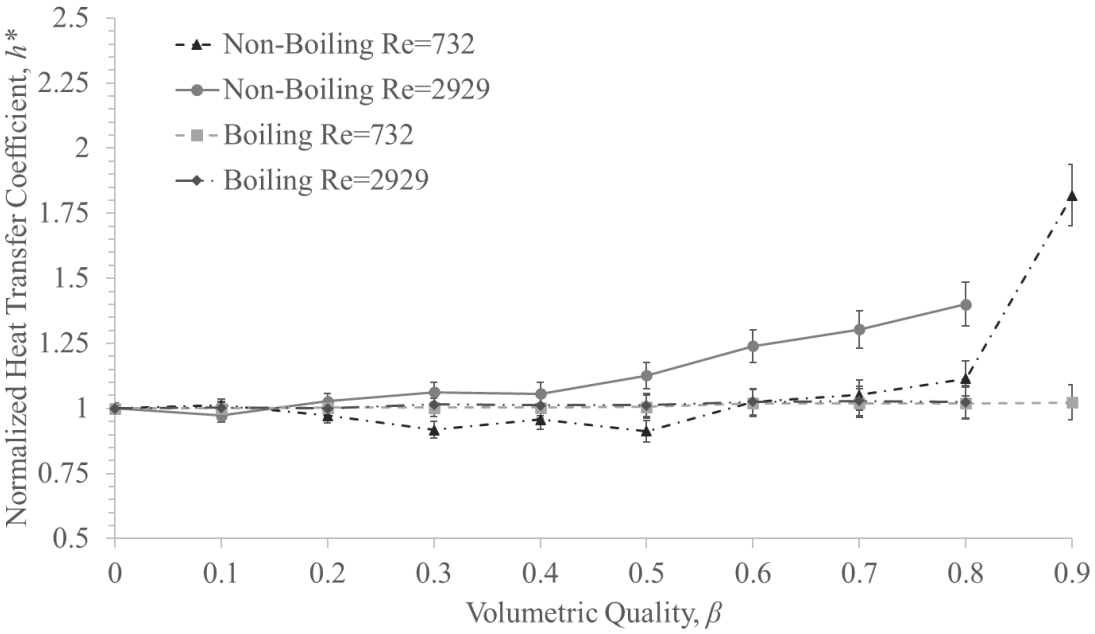

Figure 4.19: Normalized HTC showing the effects of volumetric quality on the post-wick surface.

Table 4-2: Improvements in HTC when compared to a single-phase jet.

Reynolds Number	**Plain Surface**		**Post-Wick Surface**	
	Non-Boiling	**Boiling**	**Non-Boiling**	**Boiling**
732	116.55%	9.50%	81.94%	2.38%
2929	41.64%	7.12%	39.96%	2.94%

Chapter 5 - Conclusion

5.1 - Summary

This research was conducted in hopes of producing a break-through in the topic of two-phase jet impingement and porous media. The non-boiling and boiling experiments within this research were performed successfully. All though the outcomes of the experiments weren't as expected, this research was still able to build on previous work and still allows for future work on this topic.

1. The non-boiling results seen from both surfaces at Re = 732 and Re = 2929 showed that the plain surface and post-wick performed similar. The effect of the two-phase jet was present with the improvement of the HTC of 116.55% at $\beta = 0.8$ on the plain surface when compared to the single-phase jet at Re = 732. This improvement was also seen on the post-wick surface with an increase of the HTC of 81.94% at $\beta = 0.9$ at the same Reynolds. Improvements were also seen with the increase in Reynolds number on each surface.
2. The boiling experiments yielded major differences between the surfaces. The boiling scenario allowed the post-wick to shine due to its controllable hydrodynamic instability wavelength and reduced wick thickness. The plain surface added a 9.50% maximum improvement in the HTC at $\beta = 0.9$ and Re = 732 over a single-phase jet. The post-wick surface only had a

maximum improvement of 2.94% at $\beta = 0.7$ and $Re = 2929$. The results showed that the added air to the impinging jet had minimal improvement to the HTC in the boiling scenario over the effects of boiling and a water jet.

5.2 - Future Work and Considerations

Future research on the topic of two-phase jet impingement and boiling media can be built on the back of this research. Looking at different porous structures other than a columnar post-wick, like mushroom post-wicks, LPS, microchannels, etc. could see improvements from this scenario. Developing methods to control bubble sizes within the two-phase jet impingement could yield interesting results when interacting with the vapor layer of the boiling surface. Using 3-D printing to control various properties of porous media could also result in improvement. As for the test setup, the addition of digital flow meters would eliminate some uncertainty in the flow rates of the water and air.

References

[1] R. D. Plant, J. Friedman and M. Z. Saghir, "A review of jet impingemnet cooling," *International Journal of Thermofluids,* vol. 17, 2023.

[2] I. Pop, T. Grosan, C. Revnic and A. V. Rosca, "Unsteady flow and heat transfer of nanofluids, hybrid nanofluids, micropolar fluids and porous media: A review," *Thermal Science and Engineering Process,* vol. 46, 2023.

[3] J. Fourier, The Analytical Theory of Heat, 1822.

[4] B. W. Webb and C. F. Ma, "Single Phase Liquid Jet Impingement Heat Transfer," *Advnace in Heat Transfer,* vol. 26, pp. 105-217, 1995.

[5] D. Trainer, J. Kim and S. J. Kim, "Heat Transfer and flow characterisitcs of air-assisted impinging water jets," *International Journal of Heat and Mass Transfer,* vol. 64, pp. 501-513, 2013.

[6] V. J. Rouse, "Comparison of heat transfer and fluid flow characteristics between submerged and free surface jet impingement for two-phase flow," 2018.

[7] A. Y. Cengal and A. J. Ghajar, Heat and Mass Transfer: Fundamentals & Applications, 5th ed., New York, New York: McGraw Hill, 2015.

[8] W. Rohsenow, "A method of correlating heat transfer data for surface boiling of liquids.," *Tans. Am. Soc. Mech. Eng.,* vol. 74, pp. 969-975, 1952.

[9] W. Rohsenow and P. Griffith, "Correlation of maximum heat flux data for boiling of saturated liquids," *Chem. Eng. Prog.,* vol. 52, p. 47, 1956.

[10] P. J. Berenson, "Film-Boiling Heat Transfer from a Horizontal Surface," *Journal of Heat Transfer,* vol. 83, no. 3, 1961.

[11] R. Lahey and F. Moody, The Thermal Hydraulics of a Boiling Water Nuclear Reactor, The Society, 1977.

[12] X. Liu, W. Zhou, Y. Bian, X. Zhao and Z. Jia, "Numerical study on the heat transfer characteristics of hydrocarbon fuel in the cooling channel filled with porous media," *International Communications in Heat and Mass Transfer,* vol. 149, 2023.

[13] J. Liu, P. Yu, Y. Li, C. Wan and D. Du, "Numerical simulation on convective heat transfer characteristics in porous media based on the digital rock technology," *International Journal of Heat and Mass Transfer,* vol. 196, 2022.

[14] Z.-H. Xuan, W.-Z. Fang, Y.-H. Lu, C. Yang and W.-Q. Tao, "Significance of the natural convection to the heat transfer of porous media: A pore-scale study," *International Journal of Heat and Mass Transfer,* vol. 222, 2024.

[15] M. Habibishandiz and M. Saghir, "A critical review of heat transfer enhancement methods in the presence of porous media, nanofluids, and microorganisms," *Thermal Science and Engineering Progress,* vol. 30, 2022.

[16] S. G. Liter and M. Kaviany, "Pool-boiling CHF enhancement by modulated porous-layer coating: theory and experiment," *International Journal of Heat and Mass Transfer,* vol. 44, no. 22, pp. 4287-4311, Nov. 2001.

[17] J. Wang and I. Catton, "Enhanced evaporation heat transfer in triangular grooves covered with a thin fine porous layer," *Applied Thermal Engineering,* vol. 21, no. 17, pp. 1721-1737, Dec. 2001.

[18] I. Pranoto, K. Leong and L. Jin, "The role of graphite foam pore structure on saturated pool boiling enhancement," *Applied Thermal Engineering,* vol. 42, pp. 163-172, Sep. 2012.

[19] M. Qian, J. Li, Z. Xiang, Z. Dong, J. Xiao and X. Hu, "Study on heat dissipation performance of a lattice porous structures under jet impingement cooling," *Case Studies in Thermal Engineering,* vol. 49, 2023.

[20] Y. Nasersharifia, M. Kaviany and G. Hwang, "Pool-boiling enhancement using multilevel modulated wick," *Applied Thermal Engineering,* vol. 137, pp. 268-276, 2018.

[21] W. A. Bevan, "An Experimental Study of Porous Mediums on Heat Transfer Characteristics Subjected to Water Jet Impingement," 2022.

[22] D. Lytle and B. Webb, "Air jet impingement heat transfer at low nozzle-plate spacings," *International Journal of Heat and Mass Transfer,* vol. 37, no. 12, pp. 1687-1697, Aug. 1994.

[23] K. Choo, B. K. Friedrich, A. W. Glaspell and K. A. Schilling, "The influence of nozzle-to-plate spacing on the heat transfer of fluid flow of submerged jet impingement," *International Journal of Heat and Mass Transfer,* vol. 97, pp. 66-69, 2016.

[24] B. Elison and B. W. Webb, "Local heat transfer to impinging liquid jets in the initially laminar, transitional, and turbulent regimes," *International Journal of Heat and Mass Transfer,* vol. 37, no. 8, pp. 1207-1216, 1994.

[25] H.-G. Kim, Y. Shah and S.-M. Kim, "Experimental investigation and analysis of two-phase flow instability of flow boiling in a mini-channel heat sink," *International Jounral of Heat and Mass Transfer,* vol. 213, 2023.

[26] Y. Lv, G. Xia, L. Cheng and D. Ma, "Experimental investigation into unstable two phase flow phenomena during f low boiling in multi-microchannels," *International Journal of Heat and Mass Transfer,* vol. 166, 2021.

[27] K. Choo and S. J. Kim, "Heat transfer and fluid flow characteristics of two-phase impinging jets," *International Journal of Heat and Mass Transfer,* vol. 53, pp. 5692-5699, 2010.

[28] B. K. Friedrich, A. W. Glaspell and K. Choo, "The effect of volumetric quality on heat transfer and fluid flow characteristics of air-assistant jet impingement," *International Journal of Heat and Mass Transfer,* vol. 101, pp. 261-266, 2016.

[29] S. N. Joshi and E. M. Dede, "Two-phase jet impingement cooling for high heat flux wide band-gap devices using multi-scale porous surfaces," *Applied Thermal Engineering,* vol. 110, pp. 10-17, 2017.

[30] M. D. Clark, J. A. Weibel and S. V. Garimella, "Identification of nucleate boiling as the dominant heat transfer mechanism during confined two-phase jet impingement," *International Journal of Heat and Mass Transfer,* vol. 128, pp. 1095-1101, 2019.

[31] S.-Y. Wu, S.-Y. Zhou, L. Xiao and J. Luo, "Two-phase flow and heat transfer of a cylinder via low-velocity jet impact," *International Journal of Heat and Mass Transfer,* vol. 220, 2024.

[32] I. Piya, A. Kumar, N. Kaewchoothong and C. Nuntadusit, "Flow and heat transfer characteristics of submerged impinging air-water jets," *International Journal of Thermal Sciences,* vol. 193, 2023.

[33] K. Anand, Study of Single, Axisymmetric Micro Jet Impingement Cooling, May 2010.

[34] H. Arastoopour, D. Gidaspow and R. W. Lyczkowski, Transport Phenomena in Multiphase Systems, Springer, 2022.